Investigating Efficiency of Engineered Water Nanostructures (EWNS) Generated via Electrospray Technique to Deactivate Surface Microbes in Livestock Barns

A Thesis Submitted to the College of Graduate and Postdoctoral Studies in partial fulfillment of the requirements for the degree of

Master of Science

in the Department of Chemical and Biological Engineering

University of Saskatchewan

By

Yuchen (Jordan) Si

Permission to use

The author has agreed that the Libraries of the University of Saskatchewan may make this thesis freely available for inspection. Moreover, the author has agreed that permission for extensive copying of this thesis for scholarly purposes may be granted by the professor(s) who supervised the thesis work recorded herein or, in their absence, by the Head of the Department of Chemical and Biological Engineering or the Dean of the College of Graduate and Postdoctoral Studies. Copying or publication or any other use of the thesis or parts thereof for financial gain without written approval by the University of Saskatchewan is prohibited. It is also understood that due recognition will be given to the author of this thesis and to the University of Saskatchewan in any use of the material of the thesis.

Requests for permission to copy or to make other use of material in this thesis in whole or in part should be addressed to:

Head of the Department of Chemical and Biological Engineering

57 Campus Drive

University of Saskatchewan

Saskatoon, Saskatchewan S7N 5A9 Canada

OR

Dean

College of Graduate and Postdoctoral Studies

University of Saskatchewan

116 Thorvaldson Building, 110 Science Place

Saskatoon, Saskatchewan S7N 5C9 Canada

Abstract

Electrospray has been studied for more than two centuries in applications such as drug delivery and air purification, and to study basic principles behind mass spectrometry electrohydrodynamic atomization.

More recently, electrospray systems have been used to generate engineered water nanostructures (EWNS). EWNS are generated by concurrently electrospraying and ionizing water. During the production of EWNS, reactive oxygen species (ROS) are generated, these ROS have the ability to deactivate bacteria. As such, EWNS may be a promising chemical free surface decontamination method.

The objective of the research work was to determine the optimal operating condition that produced the highest deactivation efficiency of prevalent bacteria in livestock barns. Pathogenic bacteria in livestock barns contribute to animal and human illness and disease, and a non-chemical decontaminating method, such as EWNS, would benefit the industry. To date there is no research investigating the optimal parameters for EWNS efficiency to deactivate bacteria. Parameters under study included the effect of pH, conductivity, distance between needle tip and counter electrode, water flow rate and voltage on the performance of EWNS.

The research work was conducted in two phases. In phase I, a systematics study was undertaken to investigate the electrical current and electrosprayed area under a broad range of operating parameters including voltage level and polarity, pH, conductivity, needle tip to counter electrode distance and liquid flow rate. In phase II, the bacteria deactivation efficiency of EWNS for *Escherichia.coli* and poultry barn bacteria were investigated.

The optimal EWNS operating condition that produced the highest deactivation efficiency (4 logs or 99.99%) for *E.coli* was -6.6 kV, 2 cm distance between needle tip and counter electrode, 2 μL/min, pH=7, *K*=0.20 mS/cm and 25 min of exposure time. Further, the results indicated that the nanospray technology is a potential chemical-free alternative to conventional methods (e.g., chlorine spraying) in decontaminating surfaces of livestock buildings. Scaling up the technology for larger scale applications and in-barn tests are required in future research.

Acknowledgements

First of all, I would like to express my gratitude to my supervisors, Dr. Lifeng Zhang and Dr. Shelly Kirychuk, for providing me the chance to be a member of the research group and on top of that for their continuous support and guidance in overcoming numerous obstacles I have been facing through this challenging research.

I am also grateful to Dr. Bernardo Predicala and Dr. Huiqing Guo for their feedback, support and cooperation in this work which helped me to get results of better quality.

Also, I would like to thank my committee member, Dr. Catherine Niu from the Department of Chemical and Biological Engineering for providing me with valuable advice and suggestions during the research.

I also acknowledge the Graduate Teaching Scholarship received from the University of Saskatchewan and financial support from the Natural Sciences and Engineering Research Council of Canada (NSERC), Agriculture Development Fund (ADF) from the Ministry of Agriculture of Saskatchewan, and Agrivita Canada Inc.

Table of contents

List of tables

List of figures

Nomenclature

Symbol	Definition
a	Diameter of the deposited droplets (nm)
B	Unstandardized regression coefficient
C	Electric charge (C)
$C(t)$	Bacteria concentration recovered after time t of EWNS exposure (cful/mL)
$C(0)$	Bacteria concentration at t=0 after 10 min of drying prior to EWNS exposure (cfu/mL)
d	Diameter of dome (nm)
D	Droplet diameter (m)
D_d	Produced droplet size (m)
$\vec{E}$	Electric field (V/m)
$\vec{f}_e$	Electrostatic force (N)
$f(k)$	Function of fluid dielectric constant
$\vec{g}$	Gravitational constant ($m^3/(kg\ s^2)$)
$G(k)$	Function of fluid dielectric constant
h	Height of the deposited droplets (nm)
I	Current emitted (A)
k	Dielectric constant
k_I, k_d	1.66, 6.46 (constants)
K	Liquid electrical conductivity (S/m)
L	Needle tip to counter electrode distance (cm)

p	Significance level
P	Pressure (Pa)
q_e	Charge density (C/m^3)
Q	Liquid flow rate (m^3/s)
Q_{min}	Minimum feeding flow rate (mL/h)
R^2	Coefficient of determination
SEB	Standard error of coefficient
t	Time (s)
$\vec{v}$	Fluid velocity (m/s)
V	Voltage (kV)

Greek letters

Symbol	Definition
γ	Surface tension (N/m)
ε_0	Vacuum permittivity (F/m)
ε	Relative dielectric constant of the fluid
η	Viscosity (kg/(m s))
ρ	Fluid density (kg/m^3)
τ	Charge relaxation time (s)
φ	Electric potential (V)

Chapter 1 – Introduction

The presence of harmful bacteria in livestock facilities has raised concerns about the health of animals and workers. Bacteria exposure and control are extremely crucial to ensure a safe working environment in livestock facilities [1]. There have been more than ten *Escherichia coli* outbreaks recorded from 2017 to 2019 in the world according to Centers for Disease Control and Prevention [2]. Furthermore, bacteria found in livestock facility may also infect human; *E.coli* for instance, is found to have caused approximately 200 infections and 29 human hospitalizations in the United Sates during the ground beef *E.coli* outbreak [2]. Therefore, more efforts should be exerted to minimize bacteria exposure to improve livestock and worker's health.

Current disinfection methods used in livestock facilities include disinfecting with oxidizing agents (e.g. chlorine, ozone, hydrogen peroxide) [3], fogging with organic acids, and ultraviolet irradiation [4]. Recent improvements in the use of chemicals as disinfectants is the spraying of slightly acidic electrolysed water [5]. However, there are drawbacks associated with these techniques, including high energy cost, visible and invisible damage on livestock, large chemical residuals and environmental footprints, and toxicity [6].

More recently, a novel and chemical free nanotechnology-based method has been reported for foodborne bacteria inactivation, and is found to reduce bacteria up to 2.5 log [7]. In this technique, engineered water nanostructures (EWNS) are generated as aerosols through a combined process of electrospraying and ionization. These nanoscale EWNS have been found to be effective in inactivating bacteria due to the presence of reactive oxygen species (ROS). Other studies [6, 7] have shown that electrospray and ionization processes produce a large

amount of ROS, including hydroxyl and superoxide radicals, which possess strong oxidizing and microbicidal properties. Moreover, the EWNS leaves no chemical residuals as opposed to other nanoparticles and chemicals currently used for bacteria deactivation [1]. A preliminary study has shown that these water-made nanostructures are toxicologically benign [8]. In addition to the aforementioned advantages of EWNS, water spray is also commonly used in livestock facilities for cooling animals and mitigating dust levels.

1.1 Project motivation and knowledge gap

Despite considerable progress made by various researchers through the past few decades, the effects of pH (caustic or acidic) and electrolysis in water are not clear on the performance of deactivating bacteria in an electrospray system. This could be investigated by testing caustic or acidic solutions at different concentrations. By changing the pH, the physical properties including conductivity, surface tension, density, and dielectric constant would vary compared to the original ultrapure water, which has a significant impact on establishing baselines of the experiment. The ultrapure water has a pH close to 7, while a pH less than 7 is acidic, and a pH greater than 7 is alkaline. Since very low or very high pH water is extremely corrosive, the pH range applied in the experiment is from 5 to 12.

Two main chemical reactions are associated with changing the pH. When adding caustic to water, hydroxide ions will be produced; whereas adding acid to water will produce hydrogen ions. As demonstrated in the literature review section, ROS are the key source for bacteria deactivation. Among all of the ROS, the hydroxyl radicals contribute the most in this process. Hydroxyl radical is the neutral form of the hydroxide ion. Therefore, caustic addition might generate more hydroxyl radicals resulting in improved deactivating efficiency.

In addition to altering the pH, there is still a need to investigate a broader range of operating conditions, such as voltage level and flow rate, and to evaluate these effects on the droplet size and current. This knowledge is much needed to provide guidelines for pilot and commercial EWNS design and operation. Moreover, the application of EWNS for microbial surface decontamination in livestock barns has not been explored.

Overall, the research questions were:

1. Are the nano-sized droplets generated through electrospray effective in deactivating microbial prevailing in livestock barns?
2. Does higher voltage of the power supply improve bacteria deactivation?
3. Is higher pH solution more effective in deactivating bacteria compared to neutral pH?
4. Is higher conductivity solution more effective in deactivating bacteria compared to deionized water?

1.2 Research objectives

The objective of the present work was to systematically investigate the efficiency of electrospray on bacteria deactivation. Electrical current and electrosprayed area are first studied over a broad range of voltage, water flow rate, conductivity, needle tip to counter electrode distance and pH. Moreover, deactivation efficiency was tested over a wide range of voltage (-6.6, -7.6, +6.6 and +7.6 kV), needle tip to counter electrode distance (2, 3 and 4 cm), three sets of flow rates (1, 2 and 4 µL/min), and various levels of conductivity (0.06, 0.20 and 14.72 mS/cm) and pH (7, 10 and 12), to determine the optimal operating condition with the highest efficiency. *E.coli* and bacteria within poultry barn dust samples were studied for EWNS deactivation efficiency.

1.3 Organization of thesis

The work presented in this thesis resulted in three manuscripts. The thesis is written in the manuscript-based style and organized into six chapters. The introduction is presented in Chapter 1, along with knowledge gap, objectives and thesis organization. In Chapter 2, the literature review provides some background on the principle of electrospray system, ROS generation and deactivation on bacteria, as well as scaling laws to predict liquid droplet size and minimum liquid flow rate. Chapter 3 includes the first manuscript with a focus on determining the effects of different operating conditions on electrospraying including the water droplet size, current characteristics, and electrosprayed area. Chapter 4 contains the results of *E.coli* deactivation efficiency using the EWNS method and a comparison between EWNS and non-thermal plasma on *E.coli* deactivation efficacy. Chapter 5 presents the results of deactivation efficiency of bacteria found in poultry barn dust collected from the Poultry Center of the University of Saskatchewan. Finally, a summary of results, conclusions and recommendations are presented in Chapter 6. In this work, the references are provided at the end of each chapter.

1.4 References

[1] Pyrgiotakis, G., McDevitt, J., Yamauchi, T. and Demokritou, P., 2012. A novel method for bacterial inactivation using electrosprayed water nanostructures. *Journal of Nanoparticle Research*, 14(8), pp.1027-1038.

[2] Centers for Disease Control and Prevention. 2019. Outbreak of E. Coli Infections Linked to Ground Beef. [online] Available at: <https://www.cdc.gov/ecoli/2019/o103-04-19/index.html> [Accessed 4 June 2020].

[3] Zhao, T., Zhao, P., West, J., Bernard, J., Cross, H. and Doyle, M., 2006. Inactivation of Enterohemorrhagic Escherichia coli in Rumen Content- or Feces-Contaminated Drinking Water for Cattle. *Applied and Environmental Microbiology*, 72(5), pp.3268-3273.

[4] Cossu, A., Huang, K., Cossu, M., Tikekar, R., & Nitin, N. (2018). Fog, phenolic acids and UV-A light irradiation: A new antimicrobial treatment for decontamination of fresh produce. *Food Microbiology*, 76, pp.204-208. doi: 10.1016/j.fm.2018.05.013

[5] Hao, X., Li, B., Zhang, Q., Lin, B., Ge, L., Wang, C., & Cao, W. (2013). Disinfection effectiveness of slightly acidic electrolysed water in swine barns. *Journal of Applied Microbiology*, 115(3), pp.703-710. doi: 10.1111/jam.12274.

[6] Pyrgiotakis, G., Vasanthakumar, A., Gao, Y., Eleftheriadou, M., Toledo, E., DeAraujo, A., McDevitt, J., Han, T., Mainelis, G., Mitchell, R. and Demokritou, P., 2015. Inactivation of Foodborne Microorganisms Using Engineered Water Nanostructures (EWNS). *Environmental Science & Technology*, 49(6), pp.3737-3745.

[7] Vaze, N., Jiang, Y., Mena, L., Zhang, Y., Bello, D., Leonard, S., Morris, A., Eleftheriadou, M., Pyrgiotakis, G. and Demokritou, P., 2018. An integrated electrolysis – electrospray – ionization antimicrobial platform using Engineered Water Nanostructures (EWNS) for food safety applications. *Food Control*, 85, pp.151-160.

[8] Pyrgiotakis, G., McDevitt, J., Bordini, A., Diaz, E., Molina, R., Watson, C., Deloid, G., Lenard, S., Fix, N., Mizuyama, Y., Yamauchi, T., Brain, J. and Demokritou, P., 2014. A chemical free, nanotechnology-based method for airborne bacterial inactivation using engineered water nanostructures. *Environ. Sci.: Nano*, 1(1), pp.15-26.

Chapter 2 – Literature review

In the following sections, operating principles of electrospray, alternative microbial deactivation technologies, mechanism of deactivating bacteria using engineered water nanostructures (EWNS), essential correlations related to the formation of EWNS and applications of EWNS on microbial deactivation are provided.

2.1 Electrospray operating principles

To establish an electrospray system, a high voltage, which is in the range of -20 to +20 kV, is applied between a metal capillary that contains deionized water and a grounded counter electrode. The strong electric field between the two electrodes causes the formation of a conical meniscus at the tip of the capillary, which is the so-called Taylor cone [1]. Highly charged water droplets continuously break into smaller droplets from the tip of the capillary to the counter electrode primarily due to the electrical force. Meanwhile, the high electrical force causes some water molecules and air molecules (O_2) to split and can strip off electrons, resulting in production of reactive oxygen species (ROS). These are the main mechanism to inactivate bacteria and will be discussed in a later section.

Several papers have thoroughly summarized the mechanisms of the electrospray process [2]. The electrospray technique can be conveniently divided into 3 stages: droplet formation, droplet shrinkage, and ROS formation [2].

2.1.1 Droplet formation

Figure 2.1 shows all forces exerted on a droplet and the two dominating forces in the process: electrostatic force and surface tension. Deionized water is delivered to the tip of the

electrospray capillary where it experiences a high voltage electric field. First, negative voltage is applied, then negative charges from the liquid start to accumulate on the surface of the water droplet and the applied voltage pulls the water toward the counter electrode. Surface tension is to keep charges within the liquid, acting as a counter force to hold the water on the capillary [3]. Taylor cone is formed as a result of the balance between these two forces. Eventually, the surface tension is exceeded by the applied electrostatic force, and charged droplets are generated. The diameter of the formed droplets is influenced by the applied potential, the water flow rate, and water properties [2].

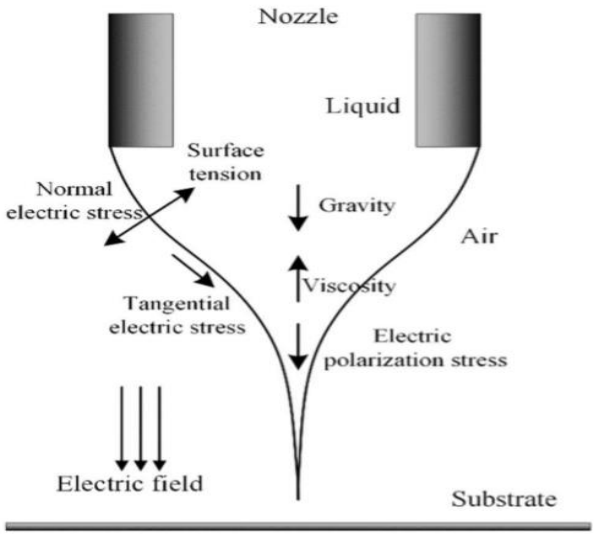

Figure 2.1 Forces exerted on the fluid from Pan and Zeng [4] (Page 3). [With permission from NCBI].

2.1.2 Droplet shrinkage

Two mechanisms are associated with droplet shrinkage. The first mechanism is that formed droplets experience evaporation due to a pressure difference which leads to a reduction in the droplet size. The second mechanism of droplet shrinkage is through fission. Fission is a process where larger droplets break into smaller droplets and it occurs when the magnitude of the charge is sufficiently high to overcome the surface tension holding the droplet together [2].

A continuous decrease in the water droplet size is mainly attributed to these two mechanisms.

2.1.3 ROS formation

In the process of electrospray and ionization, as shown in Figure 2.2 and Equations 2.1 and 2.2, some water molecules and air molecules (O_2) split or lose electrons due to the high electric field (typically around 10^6 V/m), which creates various forms of ROS including superoxide radicals (O_2^-) and hydroxyl radicals [3]. For example, Equation 2.1 shows that hydroxyl radical ($^{\bullet}OH$) is produced by free electrons accelerated to energies sufficiently high to break the chemical bonds of the water molecule after collision [5].

$$H_2O \rightarrow H^+ + {}^{\bullet}OH + e^- \quad (2.1)$$

$$O_2 + e^- \rightarrow \ O_2^- \quad (2.2)$$

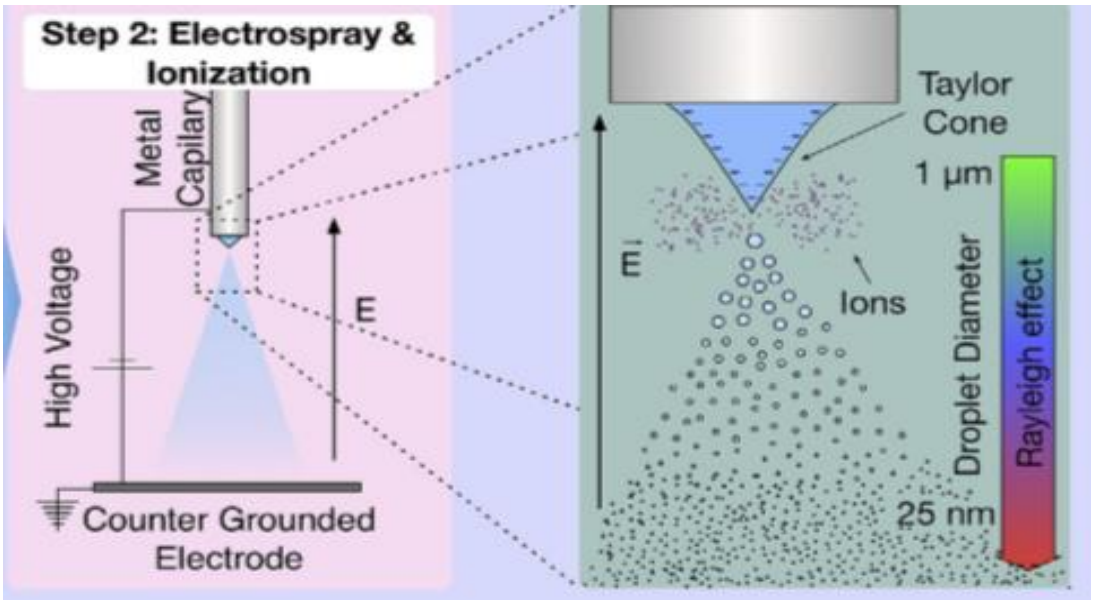

Figure 2.2 Electrospray and ionization from Vaze et al. [1] (Page 3). [With permission from Elsevier].

2.1.4 Forces applied on the water droplet

As shown in Figure 2.1, there are six forces acting on the water droplet, normal electric stress, tangential electric stress, gravity, viscosity, surface tension, and electric polarization

stress. A physical model proposed by Taylor [6] assumes that fluid is regarded as dielectric and free charges can move towards the liquid-gas interface. Cone growth and jet formation are driven by the shear forces on the interfacial charges. At the interface, the normal electric stress is balanced by the surface tension while viscous flow counterbalances the tangential components of the electric filed stress [4].

Assuming the fluid is incompressible, which corresponds to constant density and viscosity, its motion in an electric field can be described by the equations of continuity and momentum conservation as follows [4]:

$$\nabla \cdot \vec{v} = 0 \tag{2.3}$$

$$\rho \frac{d\vec{v}}{dt} = -\nabla p + \eta \nabla^2 v + \vec{f_e} + \rho \vec{g} \tag{2.4}$$

where *P* is the pressure (Pa), *t* is the time (s), $\vec{v}$ is the fluid velocity (m/s), η is fluid viscosity (kg/m) and $\vec{f_e}$ is the electromechanical force.

$$\vec{f_e} = q_e \vec{E} \tag{2.5}$$

where q_e is the charge density and $\vec{E}$ is the electric field. The charge density distribution is given by

$$q_e = \varepsilon \nabla \cdot E \tag{2.6}$$

where ε is the relative dielectric constant of the fluid. When $E = -\nabla\varphi$ and φ is the electric potential, the $\vec{f_e}$ can be expressed as follows.

$$\vec{f_e} = -\varepsilon \nabla^2 \varphi \vec{E} \tag{2.7}$$

2.1.5 The minimum flow rate through the needle

Liquid flow rate is a significant factor that determines whether the injection process can take place steadily and continuously [4]. When the flow rate is not in the proper range, Taylor

cone jet could not be formed and unstable jets, such as thin jet and thick jet, are generated [7]. Several scaling laws have been proposed for predicting the minimum flow rate required to generate the desired orientation of Taylor cones. From the two scaling laws proposed by De La Mora et al. [8] and Ganan-Calvo et al. [9] shown in Table 2.1, Ganan-Calvo's scaling law is in good agreement at high dielectric constant; whereas the one from De La Moras' agrees at low dielectric constant. Both scaling laws were summarized and compared in Chen's thesis [10].

Table 2.1 Scaling laws proposed by De La Mora et al. [8] and Ganan-Calvo et al. [9].

	Scaling laws from Fernandez De La Mora et al. [8]	Scaling laws from Ganan-Calvo et al. [9]
D_d(produced droplet size)	$G(k)(Q\tau)^{\frac{1}{3}}$	$k_d k^{\frac{-1}{6}}(Q\tau)^{\frac{1}{3}}$
I (current emitted)	$f(k)(\frac{\gamma KQ}{k})^{\frac{1}{2}}$	$k_I k^{\frac{1}{4}}(\frac{\gamma KQ}{k})^{\frac{1}{2}}$
Q_{Min}(minimum feeding flow rate)	$\frac{k\varepsilon_0\gamma}{\rho K}$	$\frac{\varepsilon_0\gamma(k)^{\frac{1}{2}}}{\rho K}$

where,

$\tau =$ charge relaxation time $(\frac{k\varepsilon_0}{K})$

$\varepsilon_0 =$ vacuum permittivity (F/m)

$\gamma =$ surface tension (N/m at 25℃)

$\rho =$ liquid density (kg/m^3)

$Q =$ liquid flow rate (m^3/s)

$K =$ liquid electrical conductivity (S/m)

$k =$ dielectric constant

$k_I, k_d = 1.66$ and 6.46 (constants)

$G(k), f(k) =$ function of fluid dielectric constant

2.2 Alternative microbial deactivation methods

At present, a few technologies have been attempted to deactivate bacteria in livestock barns, which are non-thermal plasma [11], chlorine dioxide [12] and ozone [13]. Details of the advantages and disadvantages of these technologies will be discussed and compared with EWNS in this section.

Generally, plasma refers to partially or wholly ionized gas composed essentially of photons, ions and free electrons as well as atoms in their fundamental or excited states possessing a net neutral charge [11]. For non-thermal plasma, it is often obtained under reduced pressure or atmospheric pressure and required less power. Whereas for thermal plasma, it is often obtained under a pressure higher than atmospheric pressure and required more power. The most commonly used method to generate plasma is either through corona or dielectric barrier discharge. Based on the study conducted by Misra et al. [11], the O_2 plasma is very effective in inactivating bacteria. The ROS and reactive nitrogen species (RNS) have been related to the oxidative effects on the outer surface of microbial cells. They act on the unsaturated fatty acids of the lipid bilayer of the cell membrane, impeding the transport of biomolecules across it. One key advantage of non-thermal plasma is that it acts rapidly and leaves no toxic residuals. However, short lived reactive species may not be able to last long enough to reach the bacterial surface and the effects of ultraviolet and radical species of plasma on lipids and other sensitive constituents of food are still ambiguous [11]. It may also affect the odour and flavor of meat products due to oxidation of lipid to aldehydes when it is used for food sterilization [11].

Chlorine dioxide can be used as biocide either in gaseous state or dissolves in water. In contrast to chlorine, this chlorine dioxide is effective across a broad pH range and does not

react with water, as it remains a dissolved gas in the solution. Moreover, it also does not react with ammonia or organic matter. Basically, chlorine dioxide only works for fruits with recently introduced waterborne contaminants. If the contaminants are dried, a small bath of chlorine dioxide offers little to no advantage in sanitizing fruits compared to regular tap water [12].

Ozone is a very strong oxidative chemical agent and its antimicrobial activity against a wide range of microorganisms have been studied in the past decade [13]. Ozone can destroy pesticides and chemical residuals and convert non-biodegradable organic matter to biodegradable matter. It also does not leave residuals on the contact surface. Similar to chlorine dioxide, ozone can be used to kill bacteria either in gaseous state or dissolve in water. The key problem of using gaseous ozone in an industrial scale is that it is very toxic and can be fatal for handlers if exposed for a long period of time. When compared with aqueous ozone, the solubility of ozone in water is low and the ozone concentration is higher, which might liberate into air causing safety-related hazards [13]. Corrosion is another drawback that will occur with a high concentration of ozone. Meanwhile, aqueous ozone decomposes much faster in liquid than in air and with a low concentration of ozone in water, it is not very effective [13].

2.3 Mechanism of deactivating bacteria using EWNS

The mechanism of deactivating bacteria using EWNS is through ROS lipid peroxidation [14]. Lipid peroxidation is one type of oxidative damage caused by ROS [15]. Much of the damage is caused by hydroxyl radicals generated from ROS and membrane oxidation has been detected directly in the context of bacteria [16]. Free radicals can attack polyunsaturated fatty acids directly in membranes and initiate lipid peroxidation. Mechanisms of lipid peroxidation are shown below in Figures 2.3 and 2.4. One of the main effects of lipid peroxidation is a

decrease in membrane fluidity, which alters membrane properties and can significantly disrupt membrane-bound proteins [17].

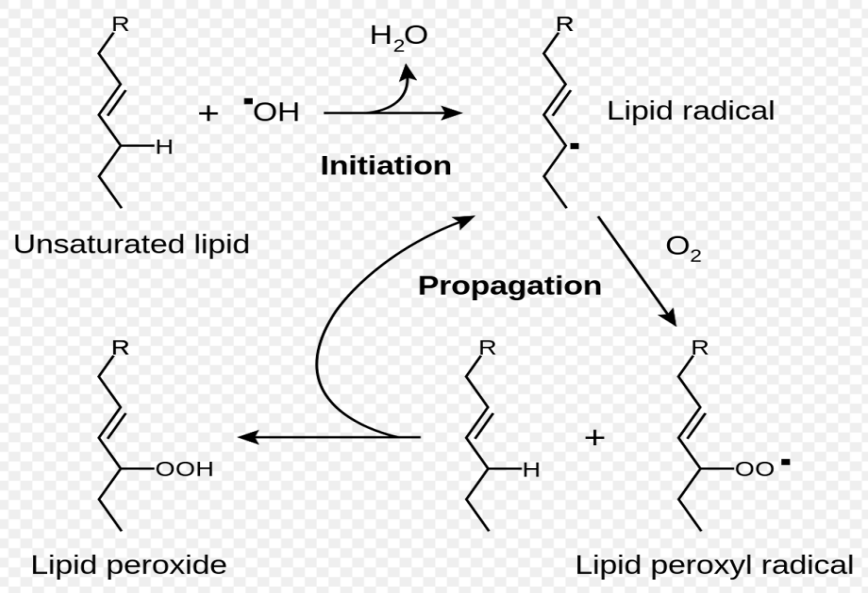

Figure 2.3 Mechanisms of lipid peroxidation from Young and McEneny [18] (Page 4). [With permission from Portland Press].

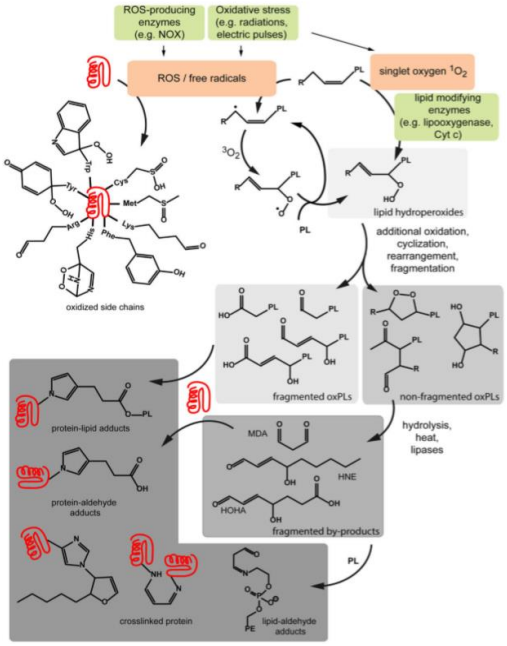

Figure 2.4 Examples of the lipid reactions from Wang et al. [16] (Page 21). [With permission from NCBI].

2.4 Other essential correlations related to the formation of EWNS

There are some useful correlations between droplet size and other operating parameters including flow rate, viscosity, and conductivity. At the same liquid flow rate, with an increase in the voltage, the current increases and the droplet size decreases based on Ganan-Calvo et al. [9]. According to Sadri et al. [19], as viscosity of the fluid increases, the droplet size as well as the size distribution increases. At the same voltage level, at a higher liquid flow rate, the velocity of the liquid increases, resulting in a decrease in charge per droplet and an increase in the droplet size. The main reason behind this effect is a reduction in the electrical force. Conductivity of the liquid also plays an important role in the droplet size. With an increase in the conductivity, the required time for charging each droplet decreases. In other words, in a given time interval, the droplet can take more charges. With more charges on the droplet, the electrical force increases, which results in formation of smaller droplets.

2.5 Applications of EWNS on microbial deactivation

Some of the potential applications of EWNS on microbial deactivation include fruit surface disinfection, surface and airborne decontamination in livestock facilities. Pyrgiotakis et al. [20] and Vaze et al. [1] have demonstrated that with *E.coli* being inoculated onto fruit surface (tomato and blackberry), 1 and 1.2 log reductions has been observed respectively by exposing the surface to the EWNS for a duration of 90 min. They have also been working on inactivating bacteria on the surface, where they use stainless-steel coupon to simulate the actual surface and achieve approximately 2.35 log reduction on deactivating *E.coli* after exposing to EWNS for a period of 45 min. When considering for airborne bacteria deactivation, it is observed that there is a 63% reduction in bacteria level [21].

2.6 References

[1] Vaze, N., Jiang, Y., Mena, L., Zhang, Y., Bello, D., Leonard, S., Morris, A., Eleftheriadou, M., Pyrgiotakis, G. and Demokritou, P., 2018. An integrated electrolysis – electrospray – ionization antimicrobial platform using Engineered Water Nanostructures (EWNS) for food safety applications. *Food Control*, 85, pp.151-160.

[2] Gaskell, S., 1997. Electrospray: Principles and Practice. *Journal of Mass Spectrometry*, 32(7), pp.677-688. doi: 10.1002/(sici)1096-9888(199707)32:7<677: aid-jms536>3.3.co;2-7.

[3] Pyrgiotakis, G., McDevitt, J., Yamauchi, T. and Demokritou, P., 2012. A novel method for bacterial inactivation using electrosprayed water nanostructures. *Journal of Nanoparticle Research*, 14(8), pp.1027-1038.

[4] Pan, Y., & Zeng, L., 2019. Simulation and Validation of Droplet Generation. Process for Revealing Three Design Constraints in Electrohydrodynamic Jet Printing. *Micromachines*, 10(2), pp.94-101. doi: 10.3390/mi10020094.

[5] Jaworek, A., Gañán-Calvo, A. and Machala, Z., 2019. Low temperature plasmas and electrosprays. *Journal of Physics D: Applied Physics*, 52(23), p.233001.

[6] Sir Geoffrey, Taylor., 1964. Disintegration of water drops in an electric field. Proceedings of The Royal Society of London. Series A. *Mathematical and Physical Sciences*, 280(1382), pp.383-397. doi: 10.1098/rspa.1964.0151

[7] Yu, M., Ahn, K., & Lee, S., 2016. Design optimization of ink in electrohydrodynamic jet printing: Effect of viscoelasticity on the formation of Taylor cone jet. *Materials & Design*, 89, pp.109-115. doi: 10.1016/j.matdes.2015.09.141.

[8] De La Mora, J. and Loscertales, I., 1994. The current emitted by highly conducting Taylor cones. *Journal of Fluid Mechanics*, 260, pp.155-184.

[9] Gañán -Calvo, A. M., Davila, J. and Barrero, A., 1994a. The emitted current and droplet size laws in steady cone-jet electrosprays of polar and non-polar liquids. Proc. 4th Int. Aerosol Con& 29 August-2 September, Los Angeles, CA.

[10] Chen, Da-Ren., 1996. Nanometer aerosol generation and measurement. Thesis (Ph. D.) -- University of Minnesota.

[11] Misra, N., Tiwari, B., Raghavarao, K. and Cullen, P., 2011. Nonthermal Plasma Inactivation of Food-Borne Pathogens. *Food Engineering Reviews*, 3(3-4), pp.159-170.

[12] Mathew, E., Muyyarikkandy, M., Bedell, C., & Amalaradjou, M., 2018. Efficacy of Chlorine, Chlorine Dioxide, and Peroxyacetic Acid in Reducing Salmonella Contamination in Wash Water and on Mangoes Under Simulated Mango Packinghouse Washing Operations. *Frontiers in Sustainable Food Systems*, 2, pp. 31-39.doi: 10.3389/fsufs.2018.00018

[13] Muhlisin, M., Utama, D., Lee, J., Choi, J. and Lee, S., 2016. Effects of Gaseous Ozone Exposure on Bacterial Counts and Oxidative Properties in Chicken and Duck Breast Meat. *Korean Journal for Food Science of Animal Resources*, 36(3), pp.405-411.

[14] Pyrgiotakis, G., McDevitt, J., Bordini, A., Diaz, E., Molina, R., & Watson, C., 2014. A chemical free, nanotechnology-based method for airborne bacterial inactivation using engineered water nanostructures. *Environmental Science-Nano*, 1(1), pp.15-26. doi: 10.1039/c3en00007a.

[15] Paiva, C.; Bozza, M., 2014. Are Reactive Oxygen Species Always Detrimental to Pathogens. *Antioxidants & Redox Signaling*, 20(6), pp.1000-1037.

[16] Wang, T., Libardo, M., Angeles-Boza, A. and Pellois, J., 2017. Membrane Oxidation in Cell Delivery and Cell Killing Applications. *ACS Chemical Biology*, 12(5), pp.1170-1182.

[17] Cabiscol, E., Tamarit, J. and Ros, J., 2000. Oxidative Stress in bacteria and protein damage by reactive oxygen species. *Internal Microbiol*, 3(3-8), pp.21-29.

[18] Young, I., & McEneny, J., 2001. Lipoprotein oxidation and atherosclerosis. *Biochemical Society Transactions*, 29(2), pp.358-365. doi: 10.1042/0300-5127:0290358

[19] Sadri, B., Vajdi Hokmabad, B., Esmaeilzadeh, E. and Gharraei, R., 2012. Experimental investigation of electrosprayed droplets behaviour of water and KCl aqueous solutions in silicone oil. *Experimental Thermal and Fluid Science,* 36, pp.249-255.

[20] Pyrgiotakis, G., Vasanthakumar, A., Gao, Y., Eleftheriadou, M., Toledo, E., DeAraujo, A., McDevitt, J., Han, T., Mainelis, G., Mitchell, R. and Demokritou, P., 2015. Inactivation of Foodborne Microorganisms Using Engineered Water Nanostructures (EWNS). *Environmental Science & Technology*, 49(6), pp.3737-3745.

[21] Pyrgiotakis, G., McDevitt, J., Gao, Y., Branco, A., Eleftheriadou, M., Lemos, B., Nardell, E. and Demokritou, P., 2014. Mycobacteria inactivation using Engineered Water Nanostructures (EWNS). *Nanomedicine: Nanotechnology, Biology and Medicine*, 10(6), pp.1175-1183.

Chapter 3 – Characterization of electrical current and liquid droplets deposition area in a capillary electrospray

The contents of this chapter have been submitted to the Journal of **Electrostatics**

Contribution of the MSc student

Experiments were planned and performed by Jordan Si with the guidance provided by Drs. Lifeng Zhang and Shelley Kirychuk. Drs. Lifeng Zhang and Shelley Kirychuk supervised and provided consultation during the entire experimental period as well as thesis preparation. All the writing of the submitted manuscript was done by Jordan Si with Drs. Lifeng Zhang, Shelly Kirychuk, Huiqing Guo and Bernardo Predicala providing editorial guidance regarding the style and content of the paper.

Contribution of this chapter to the overall study

In this chapter, the water droplets size was determined using an Atomic Force Microscope (AFM) and scaling law at an operating condition of 4 µL/min deionized water flow rate, a 3 cm needle tip to counter electrode distance, and -6.6 kV voltage. Also, the voltage and current characteristics were investigated at different flow rates, needle tip to counter electrode distances, pH and conductivities. In addition, water contact indicator was employed for the first time to measure and evaluate the electrosprayed area at the various operating conditions, including liquid flow rate, voltage level and polarity, needle tip to counter electrode distance, pH and conductivity.

3.1 Abstract

A comprehensive study was conducted to investigate the effects of applied voltage, distance between needle tip and counter electrode, liquid flow rate, pH and conductivity of water on the electrical current in a capillary electro-spray. Atomic Force Microscopy (AFM) was employed to measure the size distribution of water droplets, which presented a mean diameter of 299 ± 76 nm. Statistical analysis using a three-way ANOVA and nonlinear multivariate regression model were employed to study the interactions of applied voltage, distance between needle tip and counter electrode, and liquid flow rate with electrical current, as well as to develop regression equations to predict the current. It was found that the electrical current was significantly influenced by the applied voltage (0 to ±10 kV) and distance (2, 3 and 4 cm), but not by the liquid feed rate (1 to 10 µL/min) within the range investigated in this work. A water contact indicator was employed for the first time in the electrospray system to investigate the effect of parameters mentioned above on the liquid droplets deposition area. The experimental data demonstrates that increasing the distance between needle tip and counter electrode, liquid flow rate, pH, and conductivity, resulted in increased electrosprayed area.

3.2 Introduction

Atomization of liquids into fine droplets can be achieved by a high voltage system [1]. Electrospray has been studied for more than two centuries and its current applications include drug delivery, air purifying processes, ink-jet printing, and surface coating and ion sources in mass spectrometers [1]. In the literature, the mechanisms of the electrospray process have been summarized [2]. The electrospray technique can be conveniently divided into a number of stages; the three dominant stages are droplet formation, droplet shrinkage and gaseous ion

formation [2]. In typical electrospray processes, a high voltage is applied between a metal capillary and a grounded electrode. The strong electric field between the two electrodes causes charges to accumulate on the surface of the liquid and the resultant electrostatic force pulls the liquid towards the grounded electrode. Surface tension often acts to keep charges within the liquid, acting as counter forces to hold the liquid on the capillary [3]. A Taylor cone is a cone observed in the electrospraying process and is formed as the result of a balance between these two forces [4]. In brief, the fine droplet formation in an electrospray process is the result of the hydrostatic balance between the electrostatic force and surface tension [2]. Owing to the electrostatic repulsion, droplets will start to split into smaller droplets. The size of the liquid droplet varies from millimeters to nanometers, and according to published literature, the parameters investigated in the electrospray process that affect the diameter of the formed droplet include the applied potential, nozzle diameter, liquid flow rate and its physical properties [1, 2, 5-11]. Despite a great number of publications on different types of spraying modes and scaling laws, there have been relatively few studies related to the effects of electrical current on both positive and negative voltage polarities, capillary to grounded electrode distance, electrical conductivity, pH and liquid flow rate for water-based liquids. In addition, there is no literature available for sprayed area, which is an important parameter for scaling up and improving throughputs of electrospray techniques. Therefore, the objectives of the current work are to investigate the effect of applied voltage, pH, distance from needle tip to counter electrode, liquid flow rate and conductivity on electrical current and to evaluate the effective spray area under different operating conditions.

To this end, this work presents water contact indicator that are for the first time employed to evaluate and measure the electrosprayed area. A statistical analysis including three-way ANOVA and nonlinear regression model is conducted to evaluate the effect of voltage, needle tip to counter electrode distance and liquid flow rate on electrical current.

3.3. Methods and materials

3.3.1 Experimental setup

Figure 3.1 illustrates the experimental setup used in this study. The liquid flow rate was provided and varied by a syringe pump (NE-1000, New Era Pump Systems Inc., Farmingdale, USA). A 30 gauge needle with an inner diameter of 0.159 mm and an outer diameter of 0.311 mm (Metal Hub, Fisher Scientific, USA) coupled with a 2.5 mL syringe (1000 series Gas Tight, Hamilton, United States) was used with the syringe pump to supply the liquid at desired flow rates (1, 2 and 10 µL/min). The electrical conductivity of deionized water, Reverse Osmosis (RO) water and saline water (0.06, 0.20 and 13.94 mS/cm) was measured with a conductivity meter (Omega PHH-7200, ALPHAOMEGA Electronics, Spain). The pH of Reverse Osmosis (RO) water and caustic solution was measured with a pH meter (Omega PHH-7200, ALPHAOMEGA Electronics, Spain). A caustic solution with pH=9.76 was prepared by adding sodium hydroxide into RO water. Saline water with K=13.94 mS/cm was prepared by adding 1.1 g of sodium chloride into 150 mL of RO water.

A temperature and relative humidity sensor (HIH8120-021-001, Humidlcon, Honeywell, USA) was installed in the chamber and remotely connected to a laptop to continuously record data. A stainless-steel coupon with a diameter of 5 cm was placed on the top of the counter electrode, which was made of alumina (diameter of 5.85 cm and thickness of 0.1 cm). The

counter electrode and the coupon were placed on a support platform made of PVC, which was used to adjust the distance between the tip of the capillary needle to the counter electrode. Three distances were tested at 2, 3 and 4 cm, respectively. The electrometer (DM-45 Digital Multimeter, GreenLee, USA) was connected to the counter electrode to measure the total current passing through the coupon. A high voltage power supply (APM-30KIPNX, Kasuga Denkie Inc., Japan) was employed to provide a voltage in a range of -10 to +10 kV. The positive/negative port was connected to the needle and the counter electrode was grounded in order to generate the electric field.

During experiments, the high voltage (in the range of kV) applied between the two electrodes caused the formation of a conical meniscus at the tip of the capillary, known as the Taylor cone [12]. From the tip of the Taylor cone, highly charged water droplets continued to break into smaller droplets, which was called Engineered Water NanoStructures (EWNS) as they were drawn by the electrical field towards the counter electrode and impacted on the coupon.

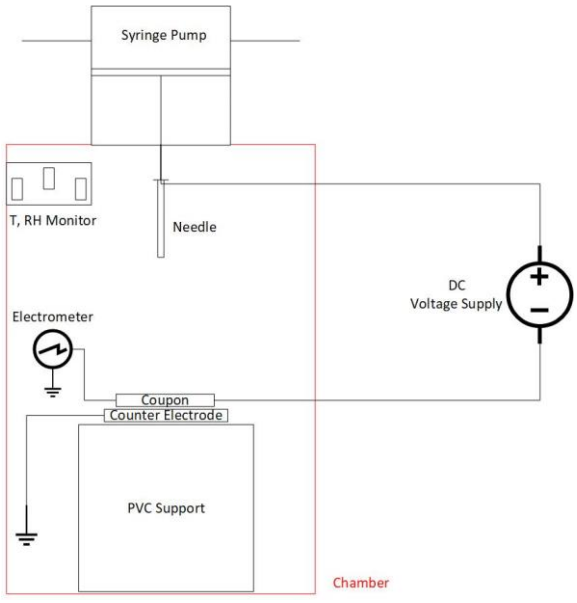

Figure 3.1 Experiment schematic.

3.3.2. Size measurement of EWNS

The Atomic Force Microscope (AFM) (4500 AFM, Keysight Technologies, USA) and the probe (Aspire CT170 probe, Nanoscience Instruments, Canada) were employed to measure the size of EWNS droplets [13]. The AFM scanned area was 14 µm x 15 µm with 512 scan lines. All images were processed by Gwyddion (an open software) and tuned to a 2nd order polynomial background. Height and diameter of the deposited droplets were measured from these processed images and they were used in Equation 3.1 below.

An electrospray setup mentioned above was used to generate EWNS at an operating condition of -6.6 kV, 4 cm distance between the needle tip and counter electrode and 4 µL/min Mili-Q water flow rate. The produced EWNS droplets were sprayed on a freshly cleaved mica surface (Great V-4 Mica, SPI Supplies, USA) for a period of 10 seconds. This duration was chosen because the water droplets were not detected when the spraying time was too short while droplet coagulation might occur when the spraying time was too long. After spraying, the mica was immediately scanned by using the AFM. With a contact angle of nearly 0° for the fresh mica, the EWNS that was deposited on the mica presented a dome shape. Therefore, Equation 3.1 was used to determine the diameter of the dome by measuring the height and the diameter of the EWNS directly from the AFM 2D image [13].

$$d = \sqrt[3]{2 \times h^2 \times (3 \times \frac{a^2 + h^2}{2 \times h} - h)} \tag{3.1}$$

where, *d* is the diameter of the dome;

a is the diameter of the deposited droplets;

h is the height of the deposited droplets;

In total, 60 EWNS droplets were measured using the AFM with an area of 14 µm x 15 µm

and the average size and size distribution were then calculated according to Equation 3.1.

3.3.3. Statistical analysis

In the electrospray experiment, there was only one measured response: current, in relation to three factors, which were the five levels of positive voltage (6, 7, 8, 9 and 10 kV)/negative voltage (-6, -7, -8, -9 and -10 kV), three levels of the needle tip to counter electrode distance (2, 3 and 4 cm) and three levels of water flow rate (1, 2 and 10 µL/min). A three-way ANOVA was tested using SPSS to determine the effects of voltage, needle tip to counter electrode distance and water flow rate on the electrical current. A significance level (p) of 0.05 was used for all statistical analysis. The mean electrical current was calculated from triplicate electrical current measurements per each factor. A nonlinear multivariate regression was performed to predict electrical current from voltage, needle tip to counter electrode distance and water flow rate. The coefficient of determination (R^2) was used to describe and measure the strength of the relationship between the model and the independent variable.

3.3.4. Electrosprayed area measurement

In this work, a water contact indicator (5557, 3M, USA) was used to measure the electrosprayed area. The color of the water contact indicator changed when in contact with water. The principle behind this idea was to electrospray the RO water on a water contact indicator that changed color from white to red when in contact with water. Then, the sprayed area could be determined by measuring the color changed area after the RO water deposited on the indicator. In order to determine the amount of time that water contact indicator was exposed to electrosprayed liquid for the color change, 45 secs, 90 secs and 180 secs of exposure time

were chosen. A photo of the water contact indicator was taken immediately after the sprayed time was reached in order to use AutoCAD to measure the sprayed area. Due to water diffusion, the area increased with the spraying time. However, it had been found that the area under the spray time of 90 seconds was the same as that observed in our separate study on microbial deactivation. In that study, Lysogeny broth (LB) agar was used as a medium to collect bacteria and after electrospraying on the agar, the sprayed area was approximately equal to the area obtained from the 90 seconds experiment. Therefore, a spray time of 90 seconds was selected to test the effect of different operating parameters on the electrosprayed area. Figure 3.2 presents water contact indicator color changes after 45 seconds and 90 seconds of electrosprayed liquid exposure time, respectively.

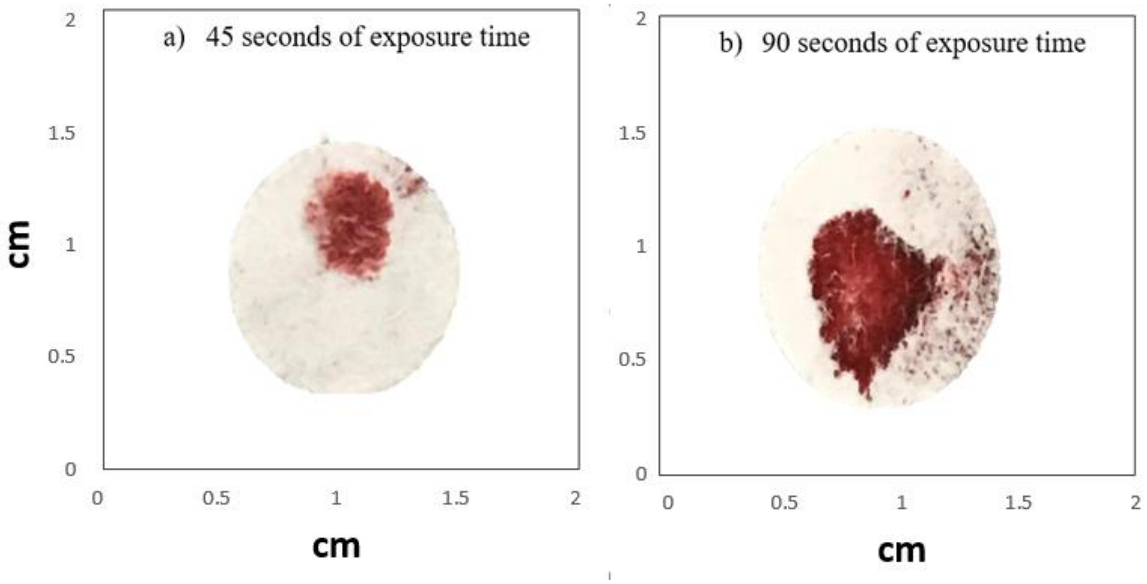

Figure 3.2 Water contact indicator color change: a) 45 seconds of exposure time. b) 90 seconds of exposure time.

3.4 Results and discussion

3.4.1 Scaling law

3.4.1.1 Minimum water feed flow rate

The liquid flow rate is an important factor that determines whether the injection process can take place steadily and continuously [14]. When the liquid flow rate is not in the proper range, the Taylor cone jet will not form and instead unstable jets, such as thin jets and thick jets, are generated [15]. A number of scaling laws have been proposed for predicting the minimum flow rate required to generate the desired orientation of Taylor cones. Of the two well-accepted scaling laws proposed by De La Mora et al. [16] and Ganan-Calvo et al. [17], the latter agrees for liquids with a high dielectric constant, whereas the former law agrees for liquids with a low dielectric constant. Both scaling laws were summarized and compared in Chen's thesis [18]. RO water has a dielectric constant of 78.36 at 25℃, which falls in the low dielectric constant category (below 100 in this case). Therefore, in this study, the minimum flow rate of RO water through a single needle electrospray was determined by using the equation by De La Mora et al. [16].

$$Q_{min} = \frac{k\varepsilon_0\gamma}{pK} \tag{3.2}$$

where, Q_{min} is the minimum water flow rate required for steady cone-jet formation;

k is the dielectric constant and =78.36 for water;

ε_0 is the vacuum permittivity and =8.85x10^{-12} F/m for water;

γ is the surface tension and =0.0728 N/m at 25℃ for water;

ρ is the density and =1000 kg/m^3 for water;

K is the liquid electrical conductivity and =0.20 mS/cm for water.

Based on the above equation, the minimum flow rate through a single needle was estimated to be 0.55 µL/min (equivalently, 0.033 mL/h). Therefore, the water flow rate chosen in this study (1 to 10 µL/min) was generally above this value.

3.4.1.2. Fine water droplet size

The scaling law of electrospray shows a functional relationship for predicting the droplet size based on experimental parameters, such as sprayed liquid properties, spray mode, applied voltage, electrodes distance and nozzle diameter. Different scaling laws have been developed based on the difference of parameters shown above. Based on the analysis rationale [19], there were six fundamental asymptotic scales combined with three conditions shown in the part of developing jet and two conditions shown in the part of cone-jet necking. These can be used to estimate the mean droplet size. Due to the sprayed liquid properties in this study (non-viscous fluid), only one asymptotic scale out of the six can be used. The droplet size scaling law with dominance of inertia and electrostatic suction was originally proposed by Ganan-Calvo et al. [8] and Hartman et al. [20] without any constraints. The droplet size can be determined as follows (Ganan-Calvo et al. [8]):

$$D = \left(\frac{\rho \varepsilon_0 Q^3}{K\gamma}\right)^{\frac{1}{6}} \tag{3.3}$$

where, D is droplet diameter;

ε_0 is the vacuum permittivity and $=8.85 \times 10^{-12}$ F/m for water;

Q is the water flow rate m^3/s.

Based on the above equation, the mean water droplet diameter was estimated to be 210 nm if a water flow rate of 2 µL/min was used.

3.4.2 EWNS size distribution

The size of EWNS is an extremely important property as it relates to the electrical mobility and surface tension exerted on the water droplets. In this study, AFM and that software was used to determine the size of EWNS after it deposited on a mica surface. Figure 3.3 shows the result of size distribution from the AFM scan after exposing the mica surface to electrospray for a period of 10 seconds. Figure 3.3a represents the AFM 3D image of EWNS depositing on a mica surface. Figure 3.3b illustrates the EWNS size distribution. Figures 3.3c and 3.3d are the 2D image of EWNS deposited on a mica surface and of a mica surface without exposing to electrospray, respectively.

It was evident from Figure 3.3d that there was no ambient particles or contaminants deposited on the controlled mica surface, which demonstrated that only EWNS droplets were presented on the mica with a mean diameter of 299 nm, a mode of 316 and a standard deviation of 76 nm (geometric standard deviation 1.29) in Figure 3.3c. When re-plugging water flow rate (4 μL/min) into Equation 3.3, the calculated mean droplet diameter was equal to 287 nm, which was consistent with the experimental value. As shown in Figure 3.3b, EWNS size distribution was rather polydisperse instead of monodisperse and this phenomenon can be attributed to several reasons, including the charge effect, Rayleigh effect and evaporation.

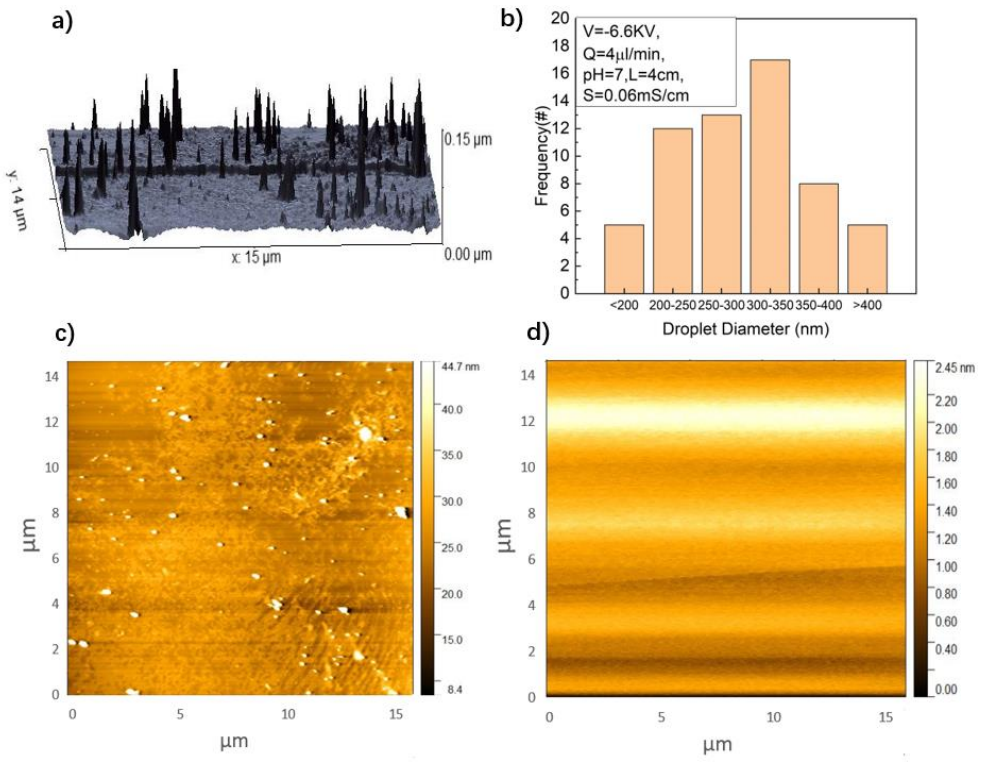

Figure 3.3 AFM measured size distribution. a) A 3D AFM image of the EWNS spreading on mica surface. b) EWNS size distribution with a mean diameter of 299 nm. c) A 2D AFM image of the EWNS spreading on mica surface. d) Controlled mica surface without exposing to EWNS.

3.4.3 V-I characteristic

3.4.3.1 Effect of voltage level and polarity

Figures 3.4 and 3.5 present the voltage-current characteristic curve of the capillary electrospray in this work. The operating range for the power supply voltage was determined to range from -10 to +10 kV because higher voltages created aggressive shaking of the needle and/or arching [13]. The gap between the needle tip and the counter electrode was set at 3 cm. An interval of 0.2 kV was applied for both negative and positive voltage starting from 0 kV. A multimeter was connected in a series with the counter electrode in order to measure the total current flowing through the stainless-steel coupon. Both figures below present the V-I relations when the water flow rate was 1 µL/min. They also present the results from the literatures with

the same flow rate and test conditions in order to compare the electrical current results with the published literature values.

Figures 3.4 and 3.5 both show that at a given voltage, the current generated by the negative voltage always lie above the positive one because of the greater mobility of the negative space charge [21]. It can be seen that corona onset voltage, which is the corona starting voltage, for positive voltage polarity occurred at about 5 kV, whereas the onset voltage was observed at about -4.4 kV for negative voltage polarity. The difference between these two values can be ascribed to new electron-ion pairs not being produced effectively for positive voltage polarity [22]. At roughly -7 KV, the slope of the V-I curve was increased and this occurrence can be described as electrical or dielectric breakdown of the air, where the electric field exceeded the dielectric strength of the air and resulted in a decrease of the resistance and an increase of the current [5]. The current in both figures shows a well-known exponential growth with respect to the power voltage and this is consistent with previous works [1, 5]. In summary, both figures below indicated that the experiment setup employed in this study was accurate and was validated by the literature values.

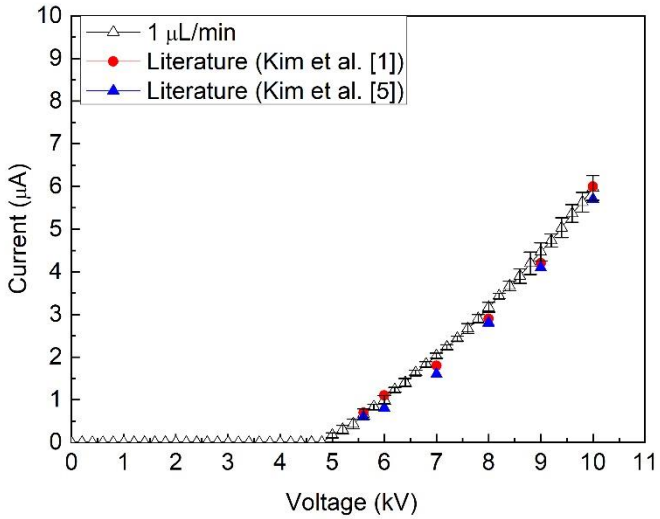

Figure 3.4 Voltage-current characteristic of the electrospray with positive voltage polarity (the nozzle inner diameter = 0.159 mm, 24°C, 30 RH%). Standard deviation of means was used to represent error bar.

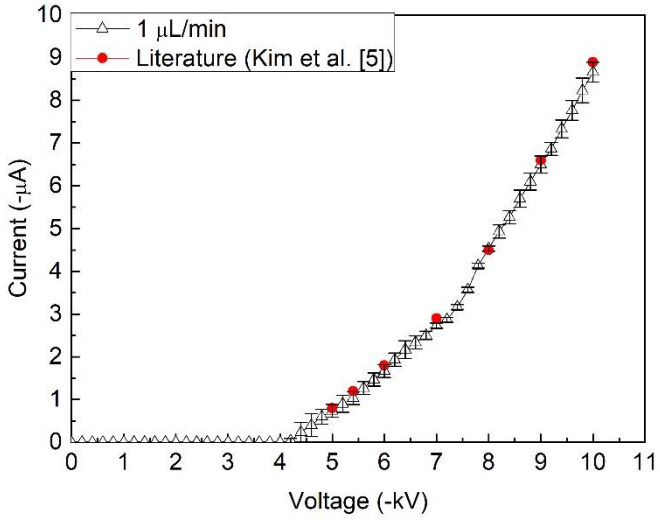

Figure 3.5 Voltage-current characteristic of the electrospray with negative voltage polarity (the nozzle inner diameter = 0.159 mm, 24°C, 30 RH%). Standard deviation of means was used to represent error bar.

3.4.3.2 Effect of distance between the needle tip and the counter electrode

As shown in Figure 3.6, for positive voltage, the current increased almost linearly with the voltage at 2, 3 and 4 cm distance between the needle tip and counter electrode. In Figure 3.7, for negative voltage, the current did not appear to increase as smoothly as the positive ones and a turning point was observed on all three curves, which could be caused by electrical breakdown of air. Sjoholm et al. [22] stated that a negative corona always accompanies with a steep growth of the electrical current with an increase in the power voltage applied. It has been shown in Figure 5 b) that the electrical breakdown occurred at a higher voltage when the distance between the needle tip and the counter electrode increased from 2 to 4 cm. The same result can also be found from Paschen's law, where the breakdown voltage depends on the composition of gas, pressure and distance between the electrodes. In summary, at a constant pressure, when the distance between the needle tip and counter electrode increased, the electric field strength decreased, so that the electrical current decreased.

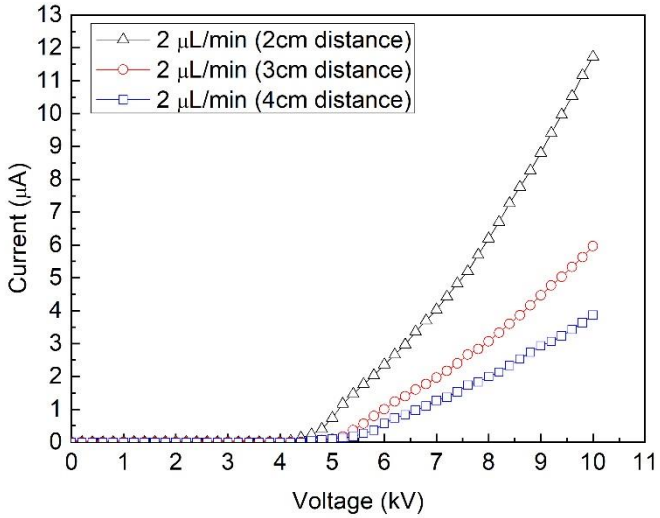

Figure 3.6 V-I characteristic curve for positive voltage polarity at different distances between needle tip and counter electrode (the nozzle inner diameter = 0.159 mm, 24°C, 30 RH%).

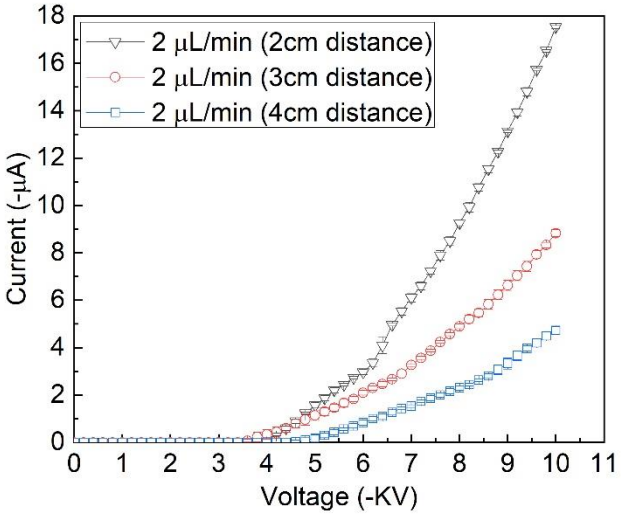

Figure 3.7 V-I characteristic curve for negative voltage polarity at different distances between needle tip and counter electrode (the nozzle inner diameter = 0.159 mm, 24°C, 30 RH%). Standard deviation of means was used to represent error bar.

3.4.3.3 Effect of water feed flow rate

The relationships of current against voltage at different flow rates are shown in Figures 3.8 and 3.9. For comparison purpose, a dry capillary case where no liquid was supplied to the needle is presented as the control. As can be seen in the two figures, three curves for the three flow rates followed the same trend and overlapped with each other regardless of negative or positive voltage applied. This implies that the resistance is only a function of the liquids' and surrounding airs' conductivity properties, and the flow rate passing through the capillary does not show an impact on the current. Jaworek et al. [23] also demonstrated that the liquid flow rate had negligible effect on the voltage – current characteristic curve. As a comparison, the current measured for the dry capillary condition showed a slightly higher value, which was also observed by Kim et al. [1]. The lower electrical current from the water spray can be attributed to the formation of charged water droplets, where these droplets have larger molecular weight than gas ions and cause a decrease in the electron's mobility [1].

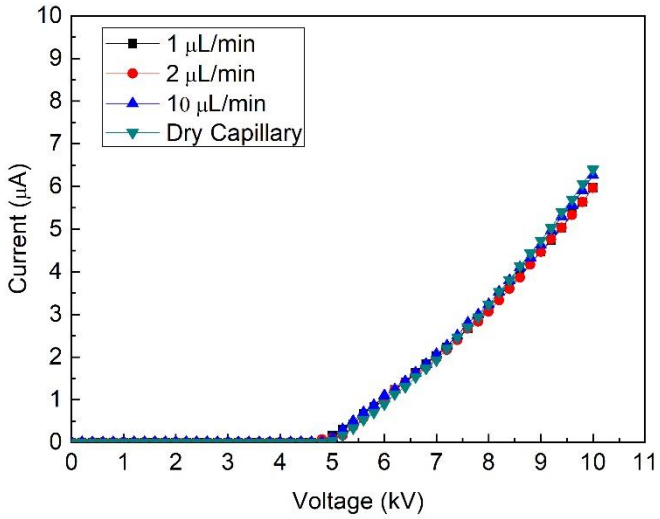

Figure 3.8 V-I characteristic curve for positive voltage polarity at different water flow rates (the nozzle inner diameter = 0.159 mm, 24°C, 30 RH%).

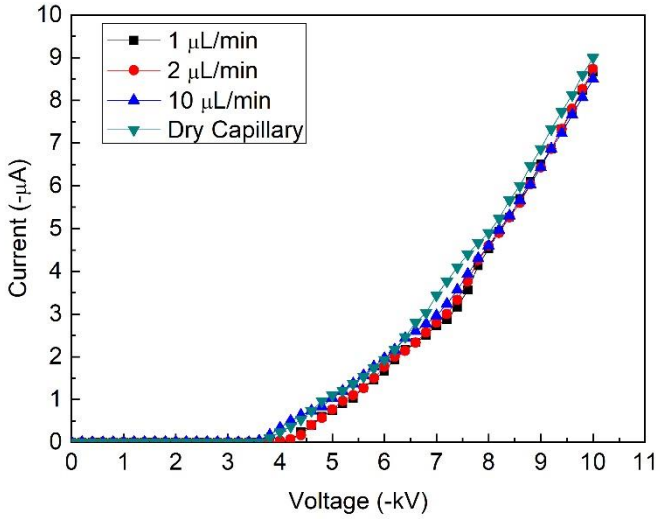

Figure 3.9 V-I characteristic curve for negative voltage polarity at different water flow rates (the nozzle inner diameter = 0.159 mm, 24°C, 30 RH%).

3.4.3.4 Effect of water pH and conductivity

Figures 3.10 and 3.11 show the voltage-current characteristic curves of electrospray for positive and negative voltage polarity at pH=7 and 9.76, respectively. Figures 3.12 and 3.13 present the voltage-current characteristic curve of the electrospray for positive and negative voltage polarity at *K*=0.20 and 13.94 mS/cm, respectively. According to the scaling law

proposed by Ganan-Calvo [8], electrical current measured in the electrospray system was a function of liquid-gas surface tension (γ) and electrical conductivity (K). By adding sodium hydroxide or sodium chloride to the water would alter the surface tension and the electrical conductivity, which would result in changes in the electrical current. In this present work, the sodium hydroxide concentration is low (0.0001M) and the effect of adding NaOH on surface tension can be neglected. As for electrical conductivity, sodium hydroxide gave out ions ($Na^+ \; and \; OH^-$) when dissolved in water, which increased the electrical conductivity to about 6 mS/cm in the solution and thereby resulted in an increase in the electrical current. For positive voltage polarity at different pH and conductivities, as the applied voltage increased, due to the addition of sodium hydroxide or sodium chloride, caustic solution and higher conductivity solution experienced more electrons movement, which resulted in higher electrical current compared to deionized water with a neutral pH and lower conductivity. However, under negative polarity, the electrical current was not increased with voltage compared to positive polarity. In both Figures 3.11 and 3.13, the electrical current at a higher pH or conductivity was about the same as the one with lower pH and conductivity, this is because more ions in the solution causes accumulation of positive space charges near the tip of the capillary, which impedes the transfer of electrons to the counter electrode [5].

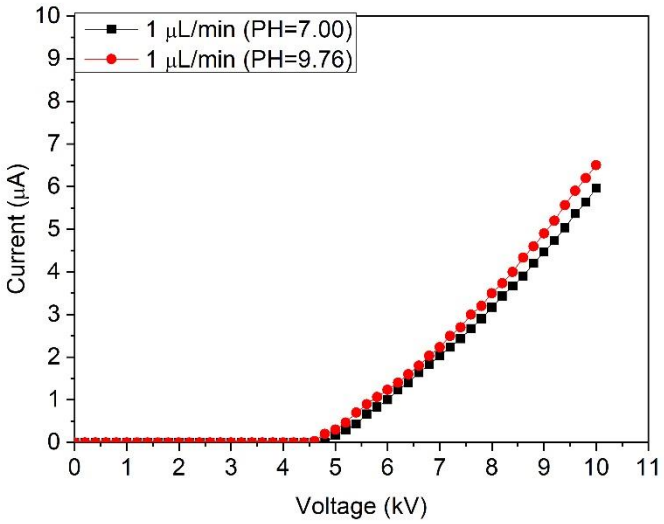

Figure 3.10 V-I characteristic curve for positive voltage polarity at different pH (the nozzle inner diameter = 0.159 mm, 24°C, 30 RH%).

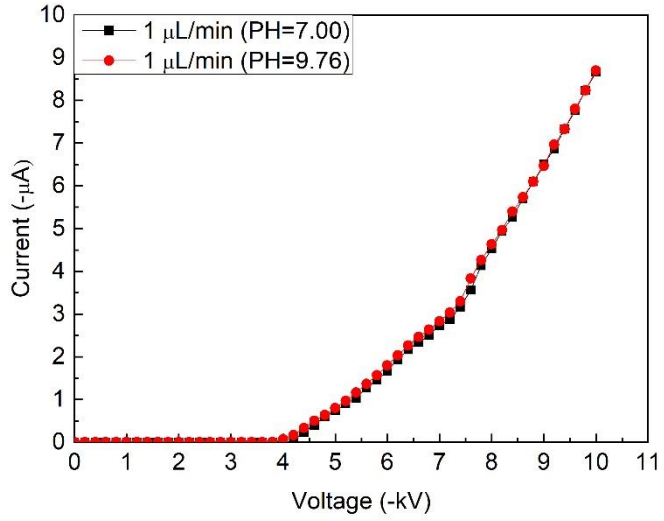

Figure 3.11 V-I characteristic curve for negative voltage polarity at different pH (the nozzle inner diameter = 0.159 mm, 24°C, 30 RH%).

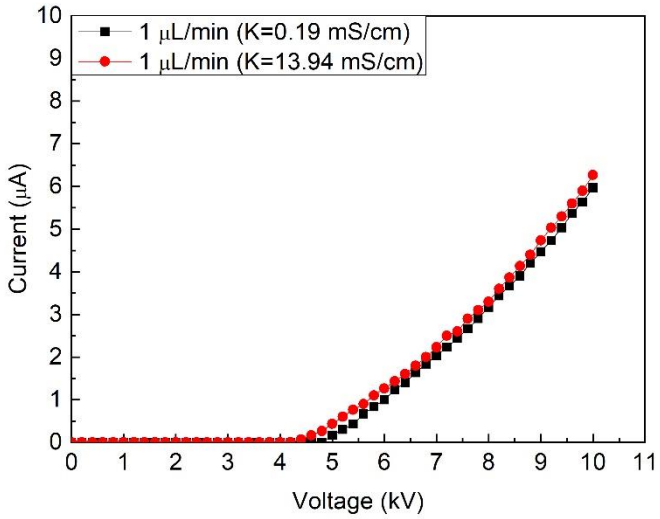

Figure 3.12 V-I characteristic curve for positive voltage polarity at different conductivity (the nozzle inner diameter = 0.159 mm, 24°C, 30 RH%).

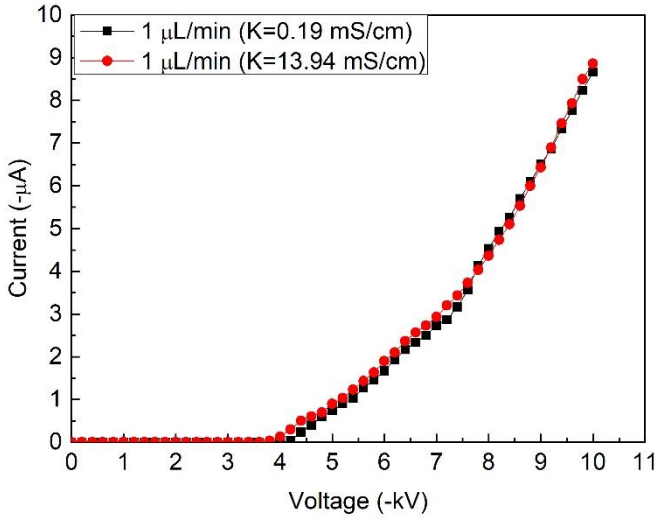

Figure 3.13 V-I characteristic curve for negative voltage polarity at different conductivity (the nozzle inner diameter = 0.159 mm, 24°C, 30 RH%).

3.4.4 Statistical analysis

3.4.4.1 Three-way ANOVA analysis

The results of three-way ANOVA statistical tests are presented in Tables 3.1 and 3.2 for positive and negative voltage, respectively. For both positive and negative voltage, it can be observed from both tables that there was no statistically significant (*p*-value= 1.000 and 0.689)

three-way interaction between both positive and negative voltage, needle tip to counter electrode distance and water flow rate, indicating that either of these parameters did not contribute to altering the electrical current. However, there were statistically significant (p<0.05) two-way interactions between positive voltage and needle tip to counter electrode distance, as well as negative voltage and needle to coupon distance, which illustrated that the relationship between voltage and electrical current depends on the needle tip to counter electrode distance. The simple main effects due to both voltage polarities and needle tip to counter electrode distance were statistically significant (p<0.05). Water flow rate illustrates no statistically significant effect (p>0.05) on the measured response in either model.

Table 3.1 Three-way ANOVA results for positive voltage

Positive Voltage Polarity Tests of Between-Subjects Effects					
Dependent Variable: Current					
Source	Type III Sum of Squares	df	Mean Square	F	Sig.
Corrected Model	1261.93[a]	44	28.68	1599.93	$p<0.001$
Intercept	2224.47	1	2224.47	124092.56	$p<0.001$
Distance	540.98	2	270.49	15089.57	$p<0.001$
Flowrate	0.00	2	7.40×10^{-5}	0.01	0.97
Voltage	602.72	4	150.68	8405.75	$p<0.001$
Distance x Flowrate	0.14	4	0.03	1.96	0.10
Distance x Voltage	117.89	8	14.73	822.11	$p<0.001$
Flowrate x Voltage	0.13	8	0.01	0.94	0.48
Distance x Flowrate x Voltage	0.04	16	0.01	0.16	1.00
Error	1.61	90	0.02		
Total	3488.02	135			
Corrected Model	1263.54	134			

[a]: $R^2=0.999$

Table 3.2 Three-way ANOVA results for negative voltage

Negative Voltage Polarity Tests of Between-Subjects Effects					
Dependent Variable: Current					
Source	Type III Sum of Squares	df	Mean Square	F	Sig.
Corrected Model	2754.82[a]	44	62.61	3213.80	p<0.001
Intercept	4465.16	1	4465.16	229200.36	p<0.001
Distance	1242.42	2	621.21	31887.38	p<0.001
Flowrate	0.01	2	0.01	0.31	0.72
Voltage	1183.83	4	295.95	15191.76	p<0.001
Distance x Flowrate	0.09	4	0.02	1.15	0.33
Distance x Voltage	327.95	8	40.99	2104.25	p<0.001
Flowrate x Voltage	0.26	8	0.03	1.69	0.11
Distance x Flowrate x Voltage	0.24	16	0.01	0.79	0.68
Error	1.75	90	0.02		
Total	7221.74	135			
Corrected Model	2756.57	134			

[a]: R^2=0.999

3.4.4.2 Nonlinear multivariate regression model

A nonlinear multivariate regression model was established based on the result of a three-way ANOVA analysis that included distance, voltage, flowrate, and the interaction terms. The nonparametric nonlinear multivariate regression model is shown below.

For positive voltage polarity, the model is presented as:

$$I = 0.15 \times e^{distance} + 3.62 \times voltage + 0.01 \times flowrate - 0.86 \times distance \times voltage - 0.03 \times distance \times flowrate + 0.05 \times voltage \times flowrate + 0.12 \times distance \times flowrate \times voltage - 11.56 \quad (3.4)$$

with a R^2 of 0.981.

For negative voltage polarity, the model is presented as:

$$I = -0.17 \times e^{distance} + 5.32 \times voltage - 0.03 \times flowrate - 0.77 \times distance \times voltage - 0.02 \times distance \times flowrate - 0.04 \times voltage \times flowrate - 0.08 \times distance \times flowrate \times voltage + 13.25 \quad (3.5)$$

with a R^2 of 0.979.

Regression coefficient and standard error of the coefficient for both models are presented in Tables 3.3 and 3.4.

Table 3.3 Positive voltage regression coefficient and standard error of the coefficient

Summary of Nonlinear Multivariate Regression Analysis		
Variable	B	SEB
Constant	-11.56	0.42
Distance	0.15	0.01
Voltage	3.62	0.06
Flowrate	0.01	0.01
Distance x Voltage	-0.86	0.02
Distance x Flowrate	-0.03	0.01
Voltage x Flowrate	0.05	0.01
Distance x Flowrate x Voltage	0.12	0.03

Note: *p<0.05; B=unstandardized regression coefficient; SEB=Standard error of coefficient

Table 3.4 Negative voltage regression coefficient and standard error of the coefficient

Summary of Nonlinear Multivariate Regression Analysis		
Variable	B	SEB
Constant	13.25	0.34
Distance	-0.17	0.01
Voltage	5.32	0.09
Flowrate	-0.03	0.01
Distance x Voltage	-0.08	0.03
Distance x Flowrate	-0.02	0.02
Voltage x Flowrate	-0.04	0.01
Distance x Flowrate x Voltage	-0.23	0.05

Note: *p<0.05; B=unstandardized regression coefficient; SEB=Standard error of coefficient

Figures 3.14 a) and b) show a comparison between the experimental values and the values predicted using nonlinear regression models. As can be observed from both figures, the current predicted by the regression models were accurately matched with the experimental values for both positive and negative voltage polarities with a R^2 of 0.981 and 0.979, respectively.

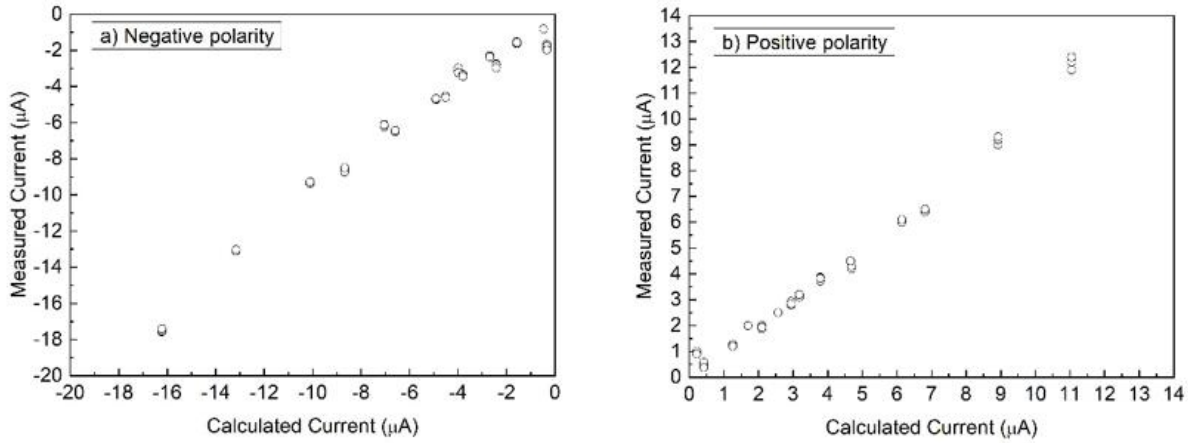

Figure 3.14 Measured and calculated current comparison: a) Negative voltage polarity. b) Positive voltage polarity.

3.4.5 Electrosprayed area

Although much effort has been devoted to developing the numerical model of the electrospray cone jet angle and jet length, very little research attention has been paid to the electrosprayed area, which is important for operating and scaling up the electrospray. In this work, water-contact indicator was employed for the first time to measure the electrosprayed area. As shown in Figure 3.15, the electrosprayed area increased with increasing exposure time. This is likely due to liquid diffusion. However, at 90 seconds exposure time, the electrosprayed area equaled 22 mm^2, which is similar to the 21 mm^2 sprayed area obtained from bacterial deactivation trials. Therefore, an exposure time was fixed at 90 seconds for investigating effects of different operating parameters on the eletrosprayed area. The opearting parameters included voltage level, needle tip to counter electrode distance, water flow rate, pH, and conductivity.

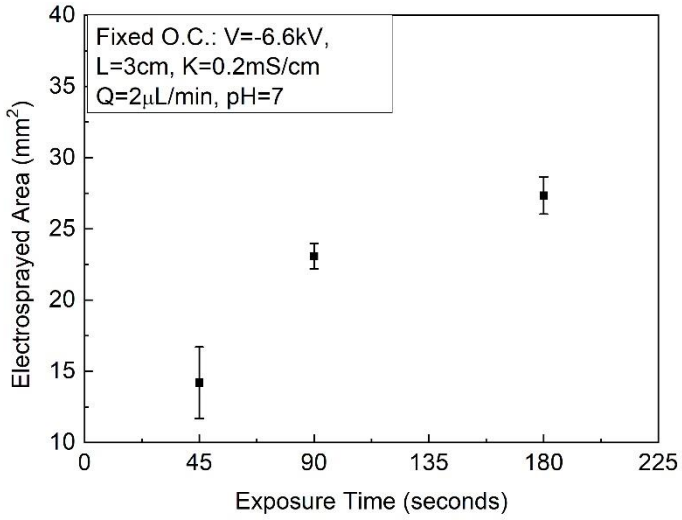

Figure 3.15 Electrosprayed area at different exposure time (Fixed O.C.= "Fixed Operating Condition"). (*V*=voltage, *L*=distance between needle tip and counter electrode, *Q*=liquid flow rate, *K*=conductivity).

3.4.5.1 Effect of voltage level and polarity on electrospayed area

Figure 3.16 illustrates the effect of the voltage change on the electrosprayed area. As shown in this figure, both -7.6 kV and -6.6 kV had a similar sprayed area, which was 23.8 mm^2 and 23.1 mm^2, respectively. However, +6.6 kV had a sprayed area of 16.7 mm^2, which was approximately 7 mm^2 smaller than those of -7.6 kV and -6.6 kV. This result is in agreement with Rosell-Llompart et al. [24] who reported that the spray cone angle is proportional to the electrical current. As demonstrated in Chapter 3.4.3, negative voltage polarity has a higher electrical current compared to the positive voltage polarity. Therefore, a larger electrosprayed area is obtained when operating at a higher voltage level and negative voltage polarity.

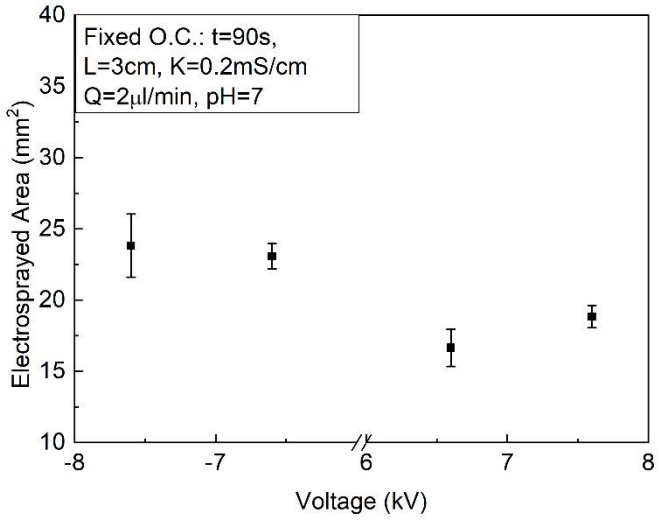

Figure 3.16 Effect of voltage level and polarity on the electrosprayed area (spray time is 90 seconds).

3.4.5.2 Effect of needle tip to counter electrode distance on electrospayed area

Figure 3.17 demonstrates the effect of change in the needle tip to counter electrode distance on the electrosprayed area. The fixed parameters in this experiment were -6.6 kV for applied voltage, 90 secs for the exposure time, 0.2 mS/cm for conductivity, 2 µL/min for water flow rate and pH=7. As shown in Figure 3.17, the electrosprayed droplets spread into a larger area

when the distance from needle tip to the counter electrode increased from 2 to 4 cm. As the distance between the needle tip to the counter electrode increased, the electric field intensity decreased, which causes increase of the dispersion of the droplets, leading to enlargement of the spray angle [25, 26].

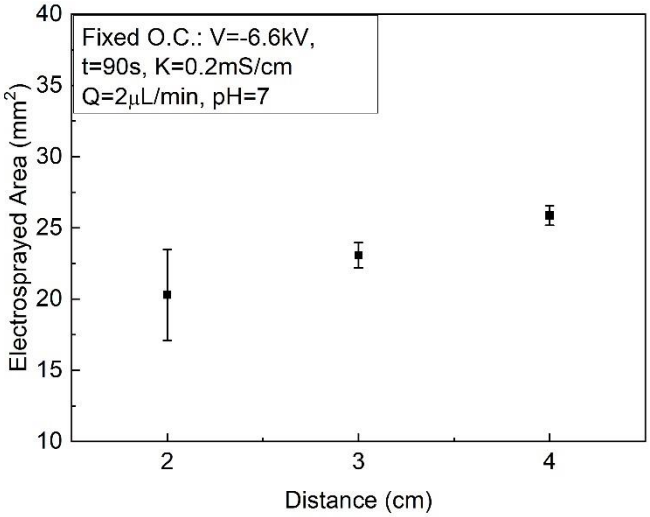

Figure 3.17 Effect of needle tip to counter electrode distance on the electrosprayed area (spray time is 90 seconds).

3.4.5.3. Effect of water flow rate on electrospayed area

Figure 3.18 shows the effect of the water flow rate on the electrosprayed area. It could be seen that the water droplets deposition area increased with increasing the liquid flow rate. At a higher liquid flow rate, more droplets will be generated and due to the same charge carried, the repulsive electrostatic force leads to an increased sprayed area.

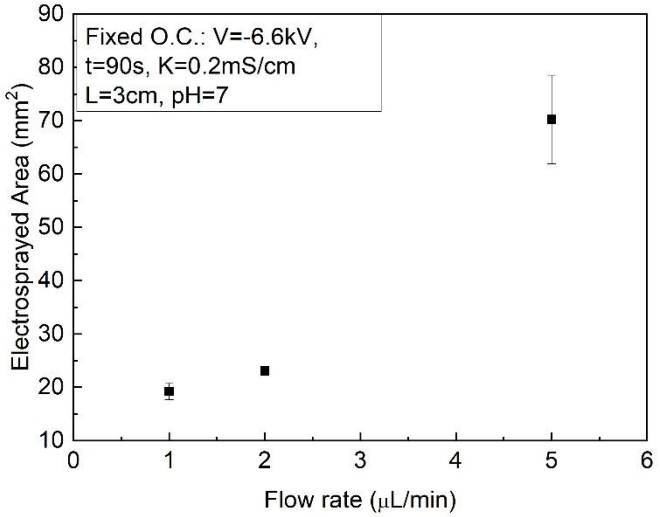

Figure 3.18 Effect of water flow rate on the electrosprayed area (spray time is 90 seconds).

3.4.5.4. Effect of pH and conductivity on electrospayed area

Figures 3.19 and 3.20 present the effect of change in pH and conductivity on the electrosprayed area, respectively. The effect of pH was clearly illustrated in Figure 3.19 where a higher pH corresponded to a higher conductivity that generated a larger spray area as compared to a neutral pH. In terms of conductivity, Mili-Q water (K=0.06 mS/cm) and RO water (K=0.20 mS/cm) had a similar sprayed area due to a small conductivity difference, but the medical grade saline water (K=13.94 mS/cm) had a sprayed area of 35 mm^2, which was 46% higher than the RO water sprayed area.Wang et al. [27] reported in their work that the spray cone (plume) angle is proportional to the electrical conductivity. Therefore, both caustic solution and medical grade saline water results a larger electrosprayed area due to their physical property (electrical conductivity).

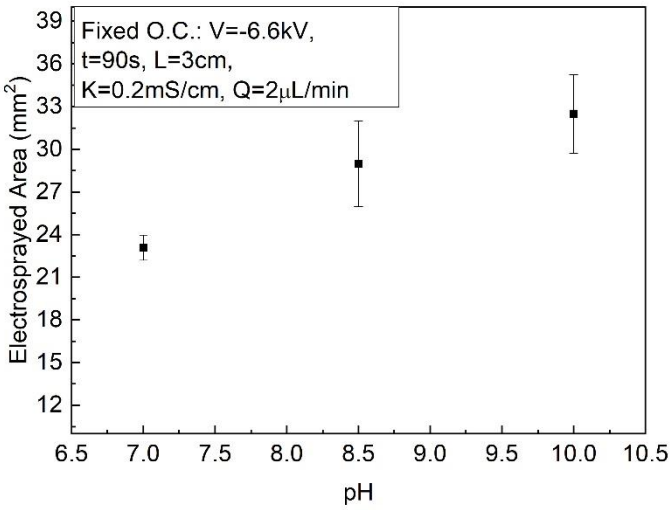

Figure 3.19 Effect of pH on the electrosprayed area (spray time is 90 seconds).

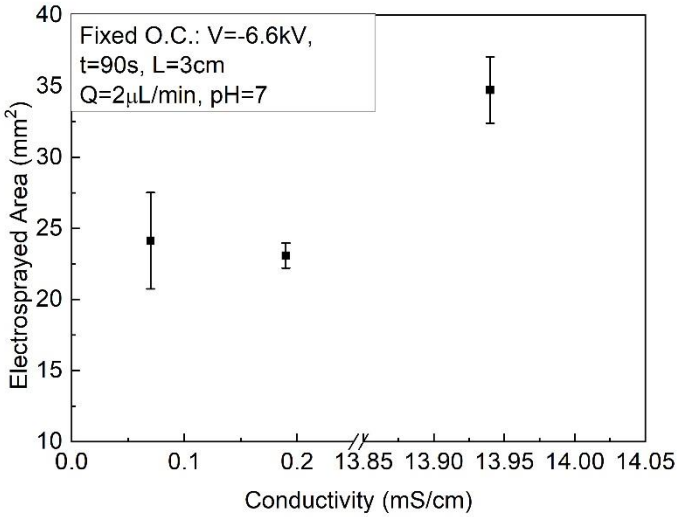

Figure 3.20 Effect of conductivity on the electrosprayed area (spray time is 90 seconds).

3.5 Conclusions

In this work, a comprehensive study was conducted to investigate the effect of applied voltage, distance between needle tip and counter electrode, water flow rate, pH and conductivity on electrical current and electrosprayed area. A three-way ANOVA and nonlinear multivariate regression model were also constructed to evaluate different parameters' interaction with electrical current. The main findings in this study can be summarized as

follows.

(1) . Within the tested range, the applied voltage and distance from needle tip to counter electrode, were the main contributing factors that affected the electrical current. The water flow rate, pH and conductivity were not significant factors.

(2) . The EWNS droplets illustrated a polydisperse droplet distribution. The mean diameter of the EWNS droplets was 299 nm, a mode of 316 nm and a standard deviation of 76 nm (geometric standard deviation 1.29), which was in the same order as compared to the other value that was calculated based on the scaling law.

(3) . The diameter of the electrosprayed area increased with increasing water flow rate, needle tip to counter electrode distance, pH and conductivity. The deposition area from a negative voltage polarity showed a larger diameter of the electrosprayed area compared to that from a positive voltage polarity. These fundamental understanding of electrosprayed area should contribute to selecting the optimum operating parameters and to enhancing the efficiency of utilizing electrosprayed droplets.

3.6 Acknowledgements

Financial support from the University of Saskatchewan and Agriculture Development Fund (ADF) from the Ministry of Agriculture of Saskatchewan, and Agrivita Canada Inc. are greatly appreciated.

3.7 References

[1] Kim, H., Kim, J. and Ogata, A., 2011. Time-resolved high-speed camera observation of electrospray. *Journal of Aerosol Science*, 42(4), pp.249-263.

[2] Gaskell, S., 1997. Electrospray: Principles and Practice. *Journal of Mass Spectrometry*, 32(7), pp.677-688.

[3] Pyrgiotakis, G., McDevitt, J., Yamauchi, T. and Demokritou, P., 2012. A novel method for bacterial inactivation using electrosprayed water nanostructures. *Journal of Nanoparticle Research*, 14(8), pp.1027-1038.

[4] Tang, K. and Gomez, A., 1995. Generation of Monodisperse Water Droplets from Electrosprays in a Corona-Assisted Cone-Jet Mode. *Journal of Colloid and Interface Science*, 175(2), pp.326-332.

[5] Kim, H., Teramoto, Y., Negishi, N., Ogata, A., Kim, J., Pongrác, B., Machala, Z. and Gañán-Calvo, A., 2014. Polarity effect on the electrohydrodynamic (EHD) spray of water. *Journal of Aerosol Science*, 76, pp.98-114.

[6] Alehosseini, A., Ghorani, B., Sarabi-Jamab, M. and Tucker, N., 2017. Principles of electrospraying: A new approach in protection of bioactive compounds in foods. *Critical Reviews in Food Science and Nutrition*, 58(14), pp.2346-2363.

[7] Biskos, G., Vons, V., Yurteri, C. and Schmidt-Ott, A., 2008. Generation and Sizing of Particles for Aerosol-Based Nanotechnology. *KONA Powder and Particle Journal*, 26(0), pp.13-35.

[8] Gañán-Calvo, A., Dávila, J. and Barrero, A., 1997. Current and droplet size in the electrospraying of liquids. Scaling laws. *Journal of Aerosol Science*, 28(2), pp.249-275.

[9] Sadri, B., Vajdi Hokmabad, B., Esmaeilzadeh, E. and Gharraei, R., 2012. Experimental investigation of electrosprayed droplets behaviour of water and KCl aqueous solutions in silicone oil. *Experimental Thermal and Fluid Science*, 36, pp.249-255.

[10] Vajdi Hokmabad, B., Sadri, B., Charan, M. and Esmaeilzadeh, E., 2012. An experimental investigation on hydrodynamics of charged water droplets in dielectric liquid medium in the presence of electric field. *Colloids and Surfaces A: Physicochemical and Engineering Aspects*, 401, pp.17-28.

[11] Xie, J., Jiang, J., Davoodi, P., Srinivasan, M. and Wang, C., 2015. Electrohydrodynamic atomization: A two-decade effort to produce and process micro-/nanoparticulate materials. *Chemical Engineering Science*, 125, pp.32-57.

[12] Vaze, N., Jiang, Y., Mena, L., Zhang, Y., Bello, D., Leonard, S., Morris, A., Eleftheriadou, M., Pyrgiotakis, G. and Demokritou, P., 2018. An integrated electrolysis – electrospray – ionization antimicrobial platform using Engineered Water Nanostructures (EWNS) for food safety applications. *Food Control*, 85, pp.151-160.

[13] Pyrgiotakis, G., Vedantam, P., Cirenza, C., McDevitt, J., Eleftheriadou, M., Leonard, S. and Demokritou, P., 2016. Optimization of a nanotechnology based antimicrobial platform for food safety applications using Engineered Water Nanostructures (EWNS). *Scientific Reports*, 6(1), pp.607-625.

[14] Pan, Y. and Zeng, L., 2019. Simulation and Validation of Droplet Generation Process for Revealing Three Design Constraints in Electrohydrodynamic Jet Printing. *Micromachines*, 10(2), pp.94-101.

[15] Yu, M., Ahn, K. and Lee, S., 2016. Design optimization of ink in electrohydrodynamic jet printing: Effect of viscoelasticity on the formation of Taylor cone jet. *Materials & Design*, 89, pp.109-115.

[16] De La Mora, J. and Loscertales, I., 1994. The current emitted by highly conducting Taylor cones. *Journal of Fluid Mechanics*, 260, pp.155-184.

[17] Gañán -Calvo, A. M., Davila, J. and Barrero, A., 1994a. The emitted current and droplet size laws in steady cone-jet electrosprays of polar and non-polar liquids. Proc. 4th Int. Aerosol Con& 29 August-2 September, Los Angeles, CA.

[18] Chen, Da Ren., 1996. Nanometer aerosol generation and measurement. Thesis (Ph. D.) -- University of Minnesota.

[19] Gañán-Calvo, A., 2004. On the general scaling theory for electrospraying. *Journal of Fluid Mechanics*, 507, pp.203-212.

[20] Hartman, R., Brunner, D., Marijnissen, J. and Scarlett, B., 1998. Scaling laws for droplet size and current produced in the cone-jet mode. *Journal of Aerosol Science*, 29, pp.S977-S978.

[21] English, W., 1948. Corona from a Water Drop. *Physical Review*, 74(2), pp.179-189.

[22] Sjoholm, P., Ingham, D., Lehtimaki, M., Perttu-Roiha, L., Goodfellow, H., Torvela, H., 13-Gas Cleaning Technology, Editor(s): Howard Goodfellow, Esko Tähti, Industrial Ventilation Design Guidebook, Academic Press, 2001, Pages 1197-1316, ISBN 9780122896767, https://doi.org/10.1016/B978-012289676-7/50016-3.

[23] Jaworek, A., Sobczyk, A., Czech, T. and Krupa, A., 2014. Corona discharge in electrospraying. *Journal of Electrostatics*, 72(2), pp.166-178.

[24] Rosell-Llompart, J., Grifoll, J. and Loscertales, I., 2018. Electrosprays in the cone-jet mode: From Taylor cone formation to spray development. *Journal of Aerosol Science*, 125, pp.2-31.

[25] Park, H., Kim, K. and Kim, S., 2004. Effects of a guard plate on the characteristics of an electrospray in the cone-jet mode. *Journal of Aerosol Science*, 35(11), pp.1295-1312.

[26] Li, W., Lin, J., Wang, X., Jiang, J., Guo, S. and Zheng, G., 2018. Electrospray deposition of ZnO thin films and its application to gas sensors. *Micromachines*, 9(2), pp.66-76.

[27] Wang, Y., Tan, M., Go, D. and Chang, H., 2012. Electrospray cone-jet breakup and droplet production for electrolyte solutions. *EPL (Europhysics Letters)*, 100(2), p.29901.

Chapter 4 – A comprehensive study of microbial deactivation by engineered water nanostructures produced by an electrospray

The contents of this chapter will be submitted to a peer-reviewed journal of publication

Contribution of the MSc student

The analytical approach was proposed by Jordan Si and Dr. Shelley Kirychuk. Calculations and data analysis were performed by Jordan Si. Dr. Lifeng Zhang supervised and provided consultation during experiments and thesis preparation.

Contribution of this chapter to the overall study

In this chapter, the *E.coli* deactivation efficiency was examined under different operating conditions, including liquid flow rate, voltage level and polarity, needle tip to counter electrode distance, EWNS exposure time, pH and conductivity. In addition, non-thermal plasma, which is another type of bacteria deactivation technology, was compared with the EWNS method on the *E.coli* deactivation efficacy.

4.1 Abstract

Electrospray is a liquid atomization process that breaks a liquid stream into a plume of highly-charged fine droplets through electrostatic forces. This technique has been successfully employed in mass spectrometry for various applications in the pharmaceutical and chemical industries. In this work, a lab-scale electrospray system using reverse osmosis (RO) water was developed to inactivate *Escherichia coli (E.coli)* that inoculated onto metal coupons. The electric field created between a needle injector (connected to a high voltage power supply) and a counter electrode (grounded) caused water droplets coming out from the needle to break into fine nano-sized droplets. The effect of applied voltage, distance between needle tip and counter electrode, liquid flow rate, exposure time, pH and conductivity on the bacteria inactivation performance were investigated to understand correlations among these parameters and to establish the optimum operating conditions for effective bacteria deactivation. Inactivation efficiency up to 4 logs was obtained under -6.6 kV, 2 cm distance between needle tip and counter electrode, 2 µL/min, pH=7, K=0.20 mS/cm and 25 min of exposure time. Results indicated that the nanospray technology is a potential chemical-free alternative to conventional methods (e.g., chlorine spraying) in decontaminating surfaces of livestock buildings. Future tests will be focused on scaling up the technology for larger scale applications.

4.2 Introduction

The presence of bacteria in livestock facilities has raised concerns about the health of animals and workers. Bacteria control and microbial decontamination is extremely crucial to ensure a safe working environment in livestock facilities [1]. There have been more than ten *Escherichia coli* outbreaks recorded from 2017 to 2019 according to Centers for Disease

Control and Prevention [2]. Further, bacteria found in livestock may also infect humans. *E.coli* for instance, was found to cause approximately 200 infections and 29 human hospitalizations in the United Sates during the ground beef *E.coli* outbreak [2]. Therefore, more efforts should be made to improve the health of livestock and farm worker and to minimize foodborne disease transmission to humans.

Microbial inactivation has become increasingly important in livestock operations. Current methods used in livestock facilities include disinfection with oxidizing agents (e.g. chlorine, ozone, hydrogen peroxide) [3], fogging with organic acids, and ultraviolet irradiation [4]. Recent improvements in the use of chemicals as disinfectants include the spraying of slightly acidic electrolysed water [5]. However, there are drawbacks to these techniques, which include high energy cost, visible and invisible damage on livestock, large chemical residuals and environmental footprints, and toxicity [6].

More recently, a novel and chemical free nanotechnology-based method has been reported for foodborne bacteria inactivation that was found to reduce bacteria up to 2.5 log [6]. In this technique, engineered water nanostructures (EWNS) are generated as aerosols through the combined process of electrospraying and ionization. These nanoscale water droplets have been found to be effective in inactivating bacteria due to the generated reactive oxygen species (ROS) embedded in the droplets. Other studies [6, 7] have shown that electrospray and ionization processes produce a large amount of ROS, including hydroxyl and superoxide radicals, which possess strong oxidizing and microbicidal properties. Moreover, the EWNS leaves no chemical residuals as opposed to other nanoparticles and chemicals currently use for bacteria deactivation [1]. In addition to the aforementioned advantages of EWNS, water spray

is also commonly used in livestock facilities for cooling animals and mitigating dust levels. Therefore, EWNS could potentially be utilized to deactivate microbes prevailing in various agriculture operations. However, a comprehensive understanding of this technique for microbial deactivation under a broad range of operating parameters (voltage level and polarity: -7.6, -6.6, 6.6 and 7.6 kV; flow rate: 1, 2 and 4 µL/min; needle tip to counter electrode distance: 2, 3 and 4 cm; pH: 7, 10 and 12; conductivity: 0.06, 0.20 and 14.72 mS/cm; exposure time: 15, 25 and 45 min) is still lacking before its wide adoptions to the food and agriculture industries.

The current study is aimed at enhancing the inactivation efficacy of EWNS droplets by varying operating parameters such as voltage levels and polarities, distances between needle tip and counter electrode, flow rate, conductivity, EWNS exposure time, and pH. The inactivation efficacies under those parameters were evaluated using a selected *E.coli* strain, which is commonly found in agriculture facilities.

4.3 Methods and materials

4.3.1 Mechanisms for the generation of engineered water nanostructures (EWNS)

In general, there are two mechanisms associated with the generation of EWNS, namely, electrospray and ionization. As shown in Figure 4.1, a high voltage (usually in the range of kilovolts) is applied to a metal capillary, which then charges the water that passes through it. The strong electric field developed between the metal capillary and the counter electrode causes formation of the so-called Taylor cone at the outlet of the capillary [6]. As the highly charged water droplets at the tip of the Taylor cone are drawn towards the counter electrode by the electric force, they continue to break into smaller droplets in a size ranging from millimeters to nanometers. According to Pyrgiotakis et al. [1], a typical nano-size water droplet normally

disappears within milliseconds due to evaporation. However, the electric charges present within the water droplets could significantly increase the surface tension and reduce the evaporation rate of the water droplets, thereby increasing their lifetime [8]. Depending on the operating conditions employed during production of EWNS aerosols, the droplet size distribution can have a diverse histogram, including monodisperse and polydisperse [6]. During the electrospray and ionization process, the high electric field causes some water molecules and air molecule (O_2) to split and lose electrons, resulting in the formation of ROS.

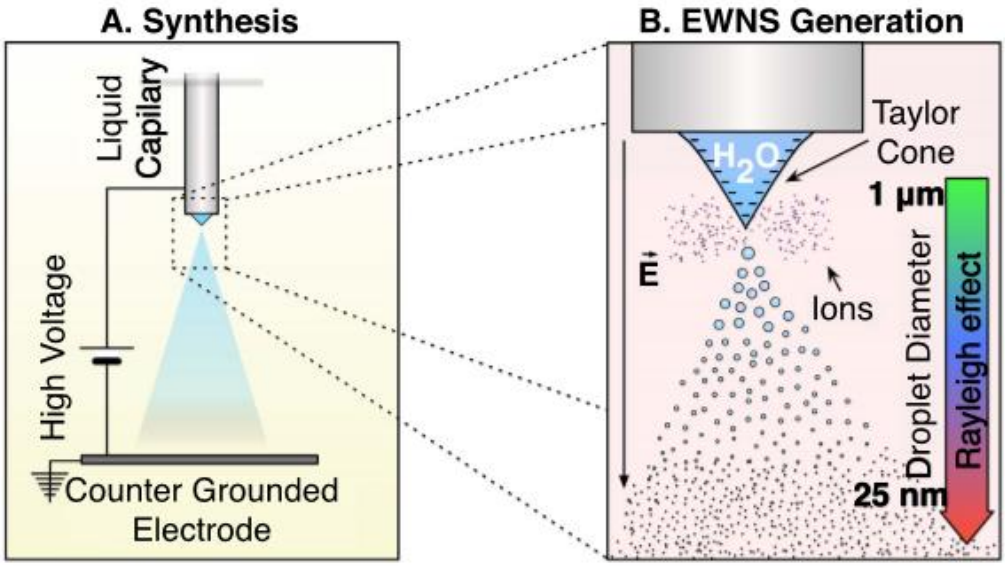

Figure 4.1 EWNS synthesis principles from Vaze et al. [6] (Page 3). A) An overview of the generation of Taylor cone and EWNS. B) Two phenomena of EWNS generation: electrospraying and ionization. [With permission from Elsevier].

4.3.2 Experimental setup

The experiments were conducted inside a Plexiglass chamber (35 cm x 35 cm x 35 cm). As shown in Figure 4.2, a syringe pump (NE-1000, New Era Pump Systems Inc., Farmingdale, USA), mounted on the top of the chamber, was used to control the liquid flow rate. In Chapter 3, it was shown that the minimum flow rate for water in order to establish a steady cone-jet formation equaled to 0.55 µL/min. With a water flow rate of 2 and 4 µL/min, the average water

droplet size was equal to 210 and 297 nm, respectively. Hence, the flow rates evaluated in this work were 1, 2 and 4 µL/min. The liquids used in this study were RO water, deionized water, saline water, and caustic solutions. The caustic solutions with pH=10 and 12 were prepared by adding sodium hydroxide into the RO water. Saline water (NaCl solution) with K=14.72 mS/cm was purchased from Fisher Scientific, Canada. The liquid was placed in a 2.5 mL syringe (1000 series Gas Tight, Hamilton, USA), which was coupled with a 30 Gauge needle (Metal Hub, Fisher Scientific, USA) with an inner diameter of 0.159 mm and an outer diameter of 0.311 mm. The electrical conductivities and pH values of the liquids were measured by a conductivity meter (Omega PHH-7200, ALPHAOMEGA Electronics, Spain) and a pH meter (Omega PHH-7200, ALPHAOMEGA Electronics, Spain). Temperature and relative humidity inside the chamber were continuously monitored using a temperature and relative humidity probe (HIH8120-021-001, Humidlcon, Honeywell, USA).

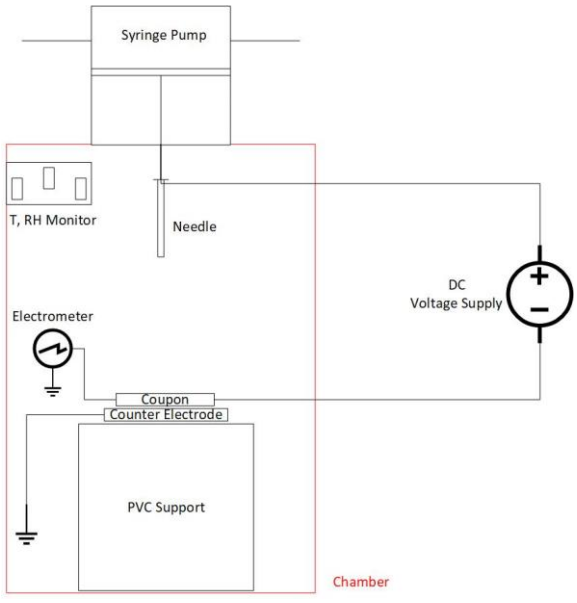

Figure 4.2 Schematic of the experiment setup.

As shown in Figure 4.2, right below the syringe needle was a 5 cm diameter stainless- steel coupon. The coupon was placed on top of a grounded counter electrode (5.85 cm in diameter

and 0.1 cm thick), which was made of alumina. Beneath the counter electrode was an adjustable polyvinyl chloride (PVC) support used to vary the distance (i.e., 2, 3 and 4 cm) between the tip of the needle and the counter electrode. The electric field within the system was generated by connecting the needle to a high voltage power supply (APM-30KIPNX, Kasuga Denkie Inc., Japan), which supplied the system voltage levels from -10 to +10 kV, and the counter electrode to the ground port of the power supply.

4.3.3 Microbial deactivation preparation

E.coli is considered to be omnipresent at farms of all types [9]. Based on the report from Centers for Disease Control and Prevention [2], there have been more than 10 recorded *E.coli* outbreak from 2017 to 2019. Therefore, in this work, *E.coli* is selected as the bacteria to evaluate the performance of EWNS on bacteria deactivation.

4.3.3.1 Preparation of *E.coli* inoculum

This study used *E.coli* (ATCC strain#27325), which was purchased from CEDARLANE, Canada. *E.coli* colonies were kept on a Lysogeny broth (LB) (DF0446-17-3, Fisher Scientific, Canada) agar at 4℃. Prior to each experiment day, one colony of *E.coli* was picked from the stock and added to 5 mL of LB medium. The culture was then incubated overnight at 37℃ in an incubator (650D, Fisher Scientific, Canada). The concentration of the bacterial solution (Eq. 4.1), which was estimated from a pre-made calibration between bacterial concentration and optical density [10]. The optical density was measured using a UV spectrophotometer (Ultrospec 3000, Pharmacia Biotech, USA) at a wavelength of 600 nm, recorded and readjusted as cfu/mL. This was used as the inoculum for further experiments.

$$E.coli\ concentration\ (\frac{cfu}{mL}) = Optical\ density\ \times 10^9 \quad (4.1)$$

4.3.3.2 Inoculation of stainless-steel coupon with *E.coli*

Prior to each experiment, the stainless-steel coupons were washed with soap solution and then thoroughly rinsed with 70% ethanol. They were then placed in a self-seal sterilization pouches (89140-800, VWR International, Canada) and autoclaved at 121℃. After autoclave, the coupons were allowed to cool in a biosafety cabinet. When cooled, 10 µL of the prepared inoculum with known concentration (1 x 10^8 cfu/mL) was placed at the center of the stainless-steel coupon. The inoculated coupon was then placed inside a closed petri dish and was allowed to dry for 10 min in the biosafety cabinet. Afterwards, the coupons inside the petri dish (with lid on) was transferred to the EWNS generation chamber.

4.3.3.3 Exposure of inoculated coupon to EWNS

The inoculated stainless-steel coupon was placed directly under the needle with its inoculated side facing the needle tip. The exposure time and all the other operating conditions employed in the study are listed in Table 4.1. Operating ranges and baseline were selected and set based on the hypothesis presented in Chapter 1 and V-I characteristic curves shown in Chapter 3. Each operating condition was performed in triplicates to ensure the accuracy of the results. All experiments were conducted at constant temperature of 20℃ and relative humidity of 25%. After each experiment, the inoculated coupon was removed from the chamber, placed again inside a closed petri dish to avoid contamination, and moved back to the biosafety cabinet for *E.coli* recovery to determine the bacteria inactivation efficacy of the EWNS.

Table 4.1 Operating conditions employed in the *E.coli* deactivation experiments.

Operating condition	Voltage (kV)	Distance between needle tip and counter electrode (cm)	Exposure time (min)	Flow rate (µL/min)	Conductivity (mS/cm)	pH
1 (Baseline)	-6.6	3	25	2	0.20	7
2	-7.6	3	25	2	0.20	7
3	6.6	3	25	2	0.20	7
4	7.6	3	25	2	0.20	7
5	-6.6	2	25	2	0.20	7
6	-6.6	4	25	2	0.20	7
7	-6.6	3	15	2	0.20	7
8	-6.6	3	45	2	0.20	7
9	-6.6	3	25	1	0.20	7
10	-6.6	3	25	4	0.20	7
11	-6.6	3	25	2	0.06	7
12	-6.6	3	25	2	14.72	7
13	-6.6	3	25	2	0.20	10
14	-6.6	3	25	2	0.20	12
15[a]	-6.6	4	15	1.2	0.06	7
16[a]	-6.6	4	30	1.2	0.06	7
17[a]	-6.6	4	45	1.2	0.06	7
18[b]	-6.6	3	25	2	N/A[d]	N/A[d]
19[c]	-6.6	3	25	N/A[d]	N/A[d]	N/A[d]

[a]Source: Vaze et al. [6].

[b]Fluid used was air instead of water.

[c]No Fluid flowing through the syringe

[d]Not applicable or no data.

4.3.3.4 Recovery of *E.coli* from inoculated coupons

After treatment with EWNS, surviving *E.coli* was recovered from the coupons by washing the coupon with 1 mL of autoclaved water and then transferring the washed water to an Eppendorf tube with proper mixing. Then, 100 µL of the washed water was withdrawn from the Eppendorf tube and plated onto LB agar plate. This step (withdrawing and plating) was performed in triplicates. All the agar plates were then placed in an incubator and incubated

overnight at 37℃ prior to colony counting. The *E.coli* concentration was also determined after 10 min of drying prior to EWNS exposure. The concentrations of *E.coli* were given in #cfu/mL.

4.3.4 Data analysis

The inactivation efficiency of EWNS produced by the electrospray was estimated through the calculation of log-reduction (Eq. 4.2) of *E.coli* from each treatment condition. The natural decay of the *E.coli* is included in Appendix D.

$$E.coli\ Deactivation\ Efficiency\ (Log) = Abs(Log_{10}(\frac{C(t)}{C(0)})) \quad (4.2)$$

where, *C(t)* is the bacteria concentration recovered after time t of EWNS exposure and *C(0)* is the bacteria concentration at t = 0, which was the time after 10 min of drying prior to EWNS exposure. Both *C(t)* and *C(0)* were obtained through recovering *E.coli* from the stainless-steel coupon after each experiment. Standard deviation of means was used to represent error bar.

4.4 Results and discussion

4.4.1 EWNS performance on inactivating *E.coli*

4.4.1.1 Comparison of EWNS performance with those published in literature

Figure 4.3 shows the inactivation rates obtained from this study and those by Vaze et al. [6], which used the same *E.coli* strain. The cited study obtained an increase in log reduction from 1.29 to 2.34 when the EWNS exposure time was increased from 15 to 45 min. Under the same operating condition (-6.6 kV, 4 cm distance between needle tip and counter electrode, 1.2 µL/min, *K*=0.06 mS/cm, pH=7) and experimental setup, log reductions from 1.61 to 2.40 was obtained in this work. This demonstrates that results from this study are comparable with those of other studies.

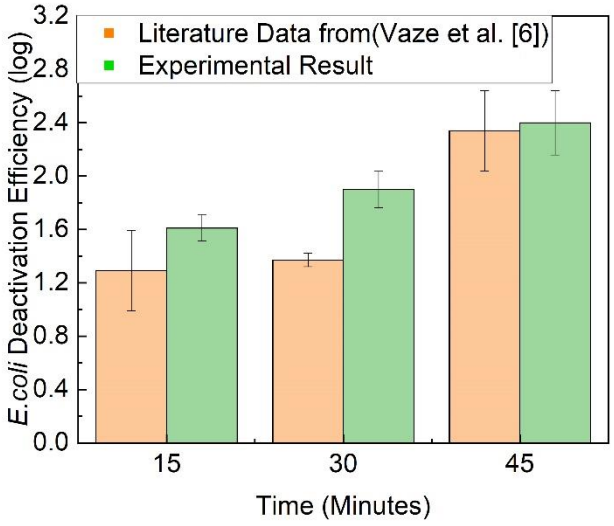

Figure 4.3 Comparison between results obtained from this study and those from Vaze et al. [6] under the following operating condition: -6.6 kV voltage, 4 cm needle tip to counter electrode distance, 1.2 µL/min flow rate, 0.06 mS/cm conductivity and pH of=7.

4.4.2 Treatment of inoculated *E.coli* with EWNS at various operating conditions

4.4.2.1 Effect of voltage level and polarity on *E.coli* inactivation efficacy

To evaluate the effect of each operating parameters on EWNS performance in inactivating *E.coli*, a sensitivity test was established and conducted by changing one operating parameter at a time while keeping the others constant. Figure 4.4 shows the *E.coli* log reductions obtained from altering the applied voltage only. The figure clearly demonstrated that with an increase in the applied voltage from -6.6 to -7.6 kV, *E.coli* inactivation efficiency increased from 2.43 log to 2.95 log. This is attributed to more ROS generated, which is the main antimicrobial species produced during the process. Ji et al. [11] found that the electron density linearly increased with increased applied voltage, which resulted in the formation of more ROS radicals. Similar results were obtained when the applied voltage was increased from +6.6 to +7.6 kV; however, the increase in *E.coli* inactivation efficiency from the negative voltage polarity was significantly higher ($p<0.05$) than those from the positive voltage polarity (Figure 4.4). This

can be due to an enhanced ROS production under negative voltage levels [12], which is facilitated by the greater mobility of the negative charges [13].

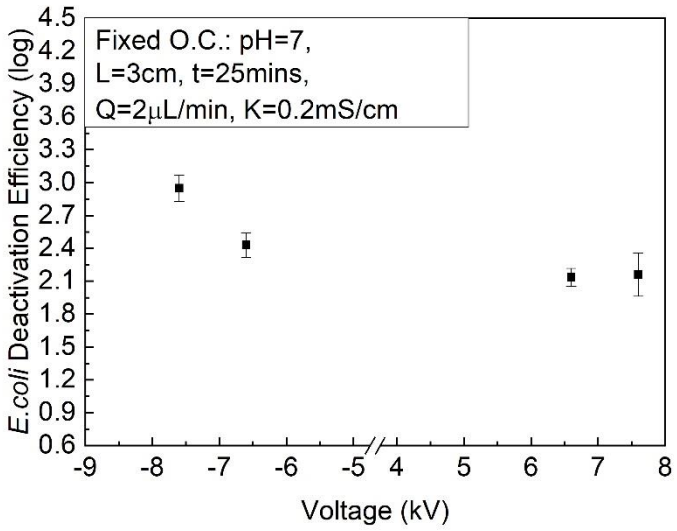

Figure 4.4 Effect of voltage level and polarity on the inactivation efficacy of *E.coli*. This employed operating conditions: 1, 2, 3 and 4 (From Table 4.1). (*L*=distance between needle tip and counter electrode, *t*=exposure time, *Q*=liquid flow rate, *K*=conductivity).

4.4.2.2 Effect of distance on *E.coli* inactivation efficacy

Figure 4.5 shows the resulting *E.coli* log reductions when the distance between the needle tip and counter electrode was changed. This employed operating condition 1(baseline), 5 and 6, which corresponded to 3, 2 and 4 cm distances (*L*), respectively. The antibacterial efficiency of EWNS was found to be the highest, which almost reached 4 log reduction, at 2 cm distance (Figure 4.5). Increasing the distance between the needle tip and counter electrode to 3 and 4 cm dramatically decreased the inactivation rates to 2.43 log and 1.23 log, respectively. This result can be explained by the theory that the quantity of electric charges (*C*) in a system is proportional to the contact time (*t*) between the electrode and fluid, and also to the discharge current (*I*) as shown in equation (4.3) [14].

$$C = I * t \tag{4.3}$$

A shorter distance between the needle tip and the counter electrode results in higher current and more electric charges as shown in Chapter 3, thus producing more ROS. This means that with more electric charges present in the system, more water molecules were oxidized to generate ROS.

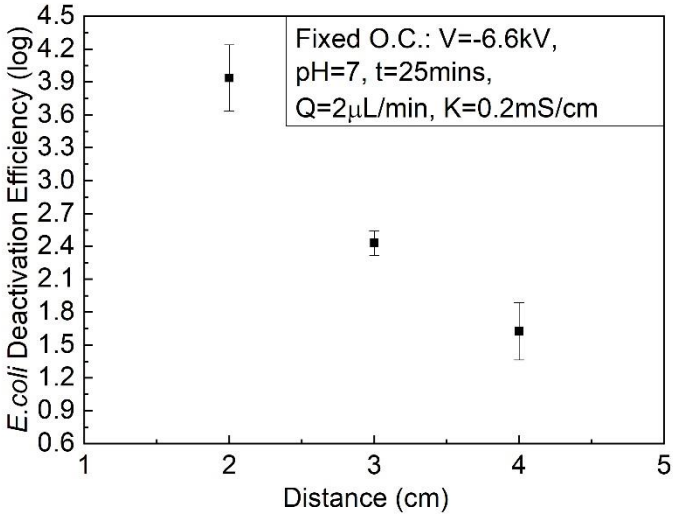

Figure 4.5 Effect of the needle tip to counter electrode distance on the inactivation efficacy of *E.coli*. This employed operating conditions: 1 (baseline), 5 and 6 (From Table 4.1).

4.4.2.3 Effect of exposure time on *E.coli* inactivation efficacy

Figure 4.6 shows the influence of exposure time to EWNS on *E.coli* inactivation efficacy. It can be seen in the figure that the inactivation efficiency increased with the exposure time to EWNS. Inactivation rates increased from 1.62 log to 3.35 log when the EWNS exposure time was increased from 15 to 45 min. It is worth noting that Vaze et al. [6] also obtained similar results. The same authors indicated that this gram-negative strain of *E.coli* experienced more protein and DNA damage at a longer exposure time. Hence, the inactivation rate of *E.coli* was higher under operating condition 8 (with exposure time of 45 min) than under the baseline

condition (with exposure time of 25 min) as more EWNS droplets could be deposited on the inoculated coupon at a longer exposure time.

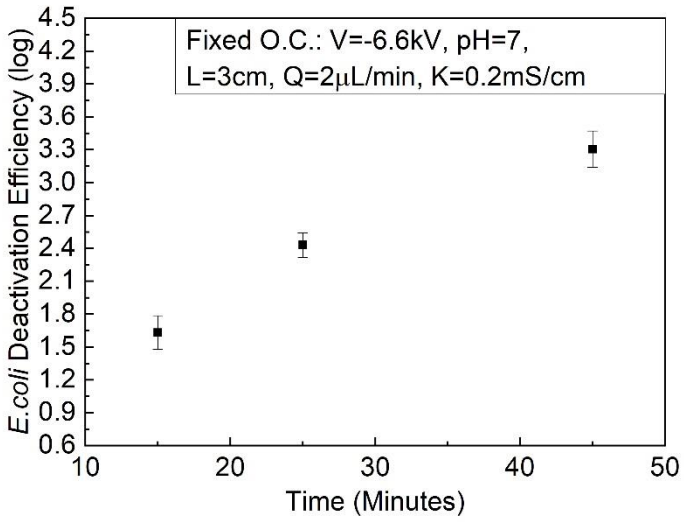

Figure 4.6 Effect of EWNS exposure time on *E.coli* inactivation efficacy. This employed operating conditions: 1 (baseline), 7 and 8 (From Table 4.1).

4.4.2.4 Effect of liquid flow rate on *E.coli* inactivation efficacy

The liquid flow rate is another operating parameter that plays a key role on the performance of EWNS in inactivating *E.coli*. As illustrated in Figure 4.7, a water flow rate of 1μL/min had the highest *E.coli* log reduction (3.03 log) compared to the other two flow rates, 2 and 4 μL/min, which resulted to 2.43 and 1.47 log reductions, respectively. This could be explained by equation (4.3), which indicates that shorter contact time between the metal capillary and the liquid, resulted in lower formation of electric charges, as well as of ROS. In Chapter 3, it also mentions that with a smaller water flow rate (ranging from 1 to 10 μL/min), the electrical current does not vary within the flow rates investigated. In addition to residence time of fluid at the capillary, slower flow rates may also result in poor stability of the electrospray [14, 15], which might be responsible for higher formation of ROS.

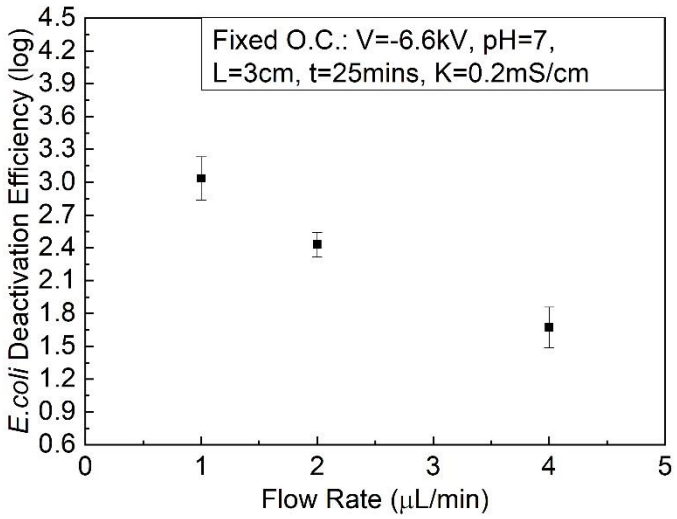

Figure 4.7 Effect of liquid flow rates on *E.coli* inactivation efficacy This employed operating conditions: 1 (baseline), 9 and 10 (From Table 4.1).

4.4.2.5 Effect of conductivity on *E.coli* inactivation efficacy

Liquid conductivity is considered one of the most significant physical properties that affect stability of electrospray and size of the sprayed droplets. Sadri et al. [16] stated that the electrospraying current increased proportionally when increasing the liquid conductivity. Equation 4.3 indicates that the electron charges are proportional with current, which implies that the higher the conductivity of the liquid, the higher the electron charges, and the better is its antimicrobial ability. Figure 4.8 illustrates the inactivation efficiencies obtained from using different types of liquid, i.e. mili-Q water, RO water, and medically-used saline water, which has conductivity values of 0.06, 0.20 and 14.72 mS/cm, respectively. Mili-Q water resulted in a 2.06 log reduction while RO water had a 2.43 log reduction. Medically-used saline water resulted in a 2.61 log reduction. The results indicate that higher conductivity leads to higher inactivation efficiency.

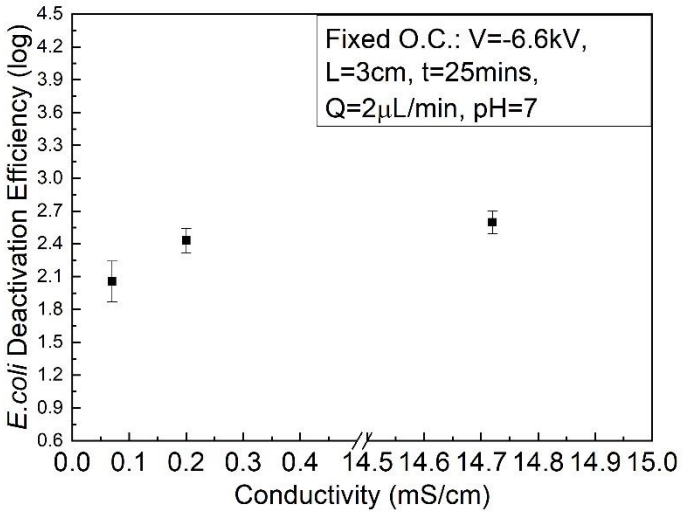

Figure 4.8 Effect of liquid conductivity on *E.coli* inactivation efficacy. This employed operating conditions: 1 (baseline), 11 and 12 (From Table 4.1).

4.4.2.6 Effect of pH on *E.coli* inactivation efficacy

Several studies [17, 18] concluded that the ROS production rate increased with an increase in liquid pH. According to Equation (4.4), hydroxide ions (OH^-) have the mechanism of converting themselves to hydroxyl radical ($^{\bullet}OH$) and electron, which indicates that a higher pH solution can produce more concentration of ROS compared to a neutral pH solution. In this study, as can be seen in Figure 4.9, a sodium hydroxide solution with a pH of 12 had a log reduction of 3.01 and it was 0.58 log higher than that of a neutral pH. This result is consistent with the finding of Sharman and Beuchat [19], which indicated that a caustic solution, in general, had an antibacterial ability, particularly for gram-negative bacteria.

$$OH^- \rightarrow {}^{\bullet}OH + e^- \qquad (4.4)$$

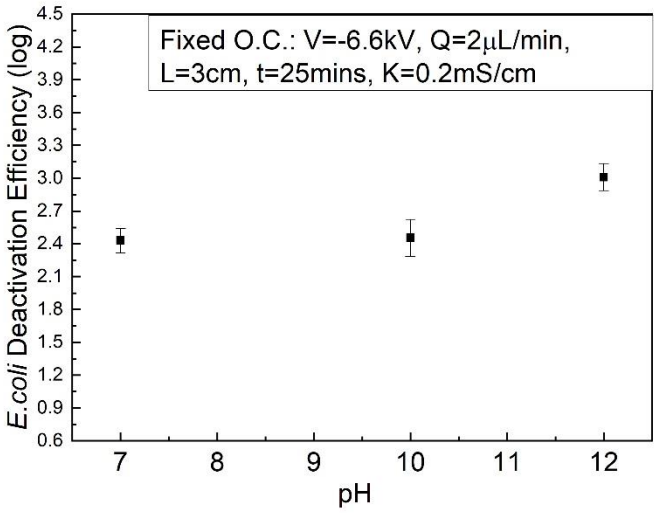

Figure 4.9 Effect of pH on *E.coli* inactivation efficacy. This employed operating conditions: 1 (baseline), 13 and 14 (From Table 4.1).

4.4.3 Comparison with non-thermal plasma and empty needle

Figure 4.10 shows that when air was used as the fluid medium (see operating condition 18), the inactivation rate was 1.53 log. This was lower than 2.43 log, which was obtained under operating condition 1 ($p<0.05$). The principle of non-thermal plasma on inactivating bacteria is the same as EWNS, as they ionized the surrounding air near the metal capillary to ROS that causes the damage on bacteria cells. The higher inactivation rate in condition 1 is mainly due to the water droplets that transports the generated ROS to the inoculated surface and surface charges on the droplet surface [1], and which prevents them from neutralizing with other air molecules, thus extending their life span from milliseconds to minutes [1].

In addition, the scenario that used an empty needle (no air or water flow) had the lowest inactivation rate (1.35 log reduction) ($p<0.05$) as there was no medium that could help diffuse the ROS to the inoculated surface.

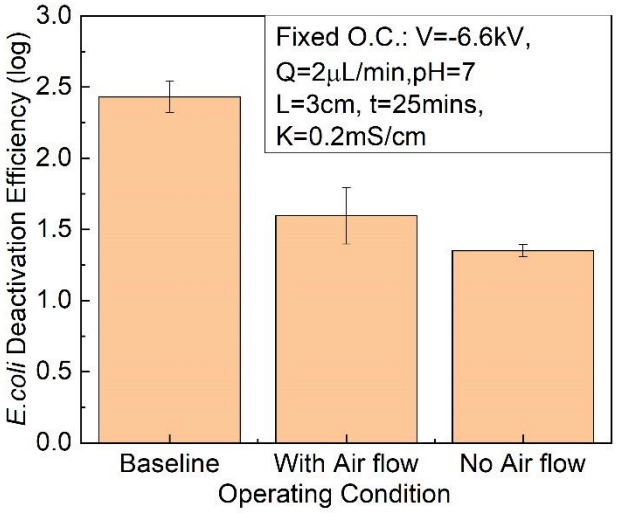

Figure 4.10 Comparison of *E.coli* inactivation rates with EWNS, non-thermal plasma and empty needle.

4.5 Conclusions

In this work, the effects of applied voltage, distance between needle tip and counter electrode, EWNS exposure time, liquid flow rate, pH and conductivity on *E.coli* inactivation rates were investigated. The main findings of this study can be summarized as follows.

(1) . It was found that higher voltage (-7.6 kV), lower liquid flow rate (1 μL/min), shorter distance between needle tip and counter electrode (2 cm), longer exposure time (45 min), and higher pH (12) and conductivity (14.72 mS/cm) resulted in higher *E.coli* inactivation rates, thus enhancing the efficiency of EWNS inactivating microbes.

(2) . Microbial deactivation efficiency is higher when EWNS is used than when non-thermal plasma and an empty needle are used.

4.6 Acknowledgements

Financial support from the University of Saskatchewan, Agriculture Development Fund (ADF) from the Ministry of Agriculture of Saskatchewan, and Agrivita Canada Inc. is greatly appreciated.

4.7 References

[1] Pyrgiotakis, G., McDevitt, J., Yamauchi, T. and Demokritou, P., 2012. A novel method for bacterial inactivation using electrosprayed water nanostructures. *Journal of Nanoparticle Research*, 14(8), pp.1027-1038.

[2] Centers for Disease Control and Prevention. 2019. Outbreak of E. Coli Infections Linked to Ground Beef. [online] Available at: <https://www.cdc.gov/ecoli/2019/o103-04-19/index.html> [Accessed 4 June 2020].

[3] A Zhao, T., Zhao, P., West, J., Bernard, J., Cross, H. and Doyle, M., 2006. Inactivation of Enterohemorrhagic Escherichia coli in Rumen Content- or Feces-Contaminated Drinking Water for Cattle. *Applied and Environmental Microbiology*, 72(5), pp.3268-3273.

[4] Cossu, A., Huang, K., Cossu, M., Tikekar, R., & Nitin, N., 2018. Fog, phenolic acids and UV-A light irradiation: A new antimicrobial treatment for decontamination of fresh produce. *Food Microbiology*, 76, pp.204-208. doi: 10.1016/j.fm.2018.05.013

[5] Hao, X., Li, B., Zhang, Q., Lin, B., Ge, L., Wang, C., & Cao, W., 2013. Disinfection effectiveness of slightly acidic electrolysed water in swine barns. *Journal of Applied Microbiology*, 115(3), pp.703-710. doi: 10.1111/jam.12274.

[6] Vaze, N., Jiang, Y., Mena, L., Zhang, Y., Bello, D., Leonard, S., Morris, A., Eleftheriadou, M., Pyrgiotakis, G. and Demokritou, P., 2018. An integrated electrolysis – electrospray –

ionization antimicrobial platform using Engineered Water Nanostructures (EWNS) for food safety applications. *Food Control*, 85, pp.151-160.

[7] Pyrgiotakis, G., Vedantam, P., Cirenza, C., McDevitt, J., Eleftheriadou, M., Leonard, S. and Demokritou, P., 2016. Optimization of a nanotechnology based antimicrobial platform for food safety applications using Engineered Water Nanostructures (EWNS). *Scientific Reports*, 6(1), pp. 607-625.

[8] Nielsen, J., Maus, C., Rzesanke, D. and Leisner, T., 2011. Charge induced stability of water droplets in subsaturated environment. *Atmospheric Chemistry and Physics*, 11(5), pp.2031-2037.

[9] De Rooij, M., Hoek, G., Schmitt, H., Janse, I., Swart, A., Maassen, C., Schalk, M., Heederik, D. and Wouters, I., 2019. Insights into Livestock-Related Microbial Concentrations in Air at Residential Level in a Livestock Dense Area. *Environmental Science & Technology*, 53(13), pp.7746-7758.

[10] Sezonov, G., Joseleau-Petit, D. and D'Ari, R., 2007. Escherichia coli Physiology in Luria-Bertani Broth. *Journal of Bacteriology*, 189(23), pp.8746-8749.

[11] Ji, W., Lee, M., Kim, G. and Kim, E., 2019. Quantitation of the ROS production in plasma and radiation treatments of biotargets. *Scientific Reports*, 9(1), pp.41-63.

[12] Nani, L., Tampieri, F., Ceriani, E., Marotta, E. and Paradisi, C., 2018. ROS production and removal of the herbicide metolachlor by air non-thermal plasma produced by DBD, DC− and DC+ discharges implemented within the same reactor. Journal of Physics D: *Applied Physics*, 51(27), p.274002.

[13] English, W., 1948. Corona from a Water Drop. *Physical Review*, 74(2), pp.179-189.

[14] Pei, J., Hsu, C., Yu, K., Wang, Y. and Huang, G., 2018. Time-resolved method to distinguish protein/peptide oxidation during electrospray ionization mass spectrometry. *Analytica Chimica Acta*, 1011, pp.59-67.

[15] McClory, P. and Håkansson, K., 2017. Corona Discharge Suppression in Negative Ion Mode Nanoelectrospray Ionization via Trifluoroethanol Addition. *Analytical Chemistry*, 89(19), pp.10188-10193.

[16] Sadri, B., Vajdi Hokmabad, B., Esmaeilzadeh, E. and Gharraei, R., 2012. Experimental investigation of electrosprayed droplets behaviour of water and KCl aqueous solutions in silicone oil. *Experimental Thermal and Fluid Science*, 36, pp.249-255.

[17] Khan, M., Philip, L., Cheung, G., Vadakepeedika, S., Grasemann, H., Sweezey, N. and Palaniyar, N., 2018. Regulating NETosis: Increasing pH Promotes NADPH Oxidase-Dependent NETosis. *Frontiers in Medicine*, 5, pp.123-142.

[18] Liu, W., Au, D., Anderson, D., Lam, P. and Wu, R., 2007. Effects of nutrients, salinity, pH and light:dark cycle on the production of reactive oxygen species in the alga Chattonella marina. *Journal of Experimental Marine Biology and Ecology*, 346(1-2), pp.76-86.

[19] Sharma, M. and Beuchat, L., 2004. Sensitivity of Escherichia coli O157:H7 to Commercially Available Alkaline Cleaners and Subsequent Resistance to Heat and Sanitizers. *Applied and Environmental Microbiology*, 70(3), pp.1795-1803.

Chapter 5 – A preliminary study of poultry barn bacteria deactivation by engineered water nanostructures produced by an electrospray

The contents of this chapter will be submitted to a peer-reviewed journal for publication

Contribution of the MSc student

The experiments, calculations and data analysis were performed by Jordan Si. Drs. Lifeng Zhang and Shelley Kirychuk supervised and provided consultation during experiments and thesis preparation.

Contribution of this chapter to the overall study

In this chapter, the bacteria collected in a poultry barn was used to determine the deactivation efficiency under different operating conditions, including liquid flow rate, voltage level and polarity, needle tip to counter electrode distance, EWNS exposure time, pH and conductivity. In addition, ozone effect was considered and tested to demonstrate that the ozone does not significantly ($p>0.05$) contribute in bacteria deactivation.

5.1 Abstract

Electrospray is a special liquid atomization process that relies on electrostatic force to break a liquid into a plume of highly charged fine droplets. This technique has been successfully employed in mass spectrometry for various applications in the pharmaceutical and chemical industries. In this study, a lab-scale electrospray system using Reverse Osmosis (RO) water was developed to inactivate bacteria collected on the Lysogeny broth (LB) agar plate in a poultry barn. The effects of applied voltage, distance between needle tip and counter electrode, liquid flow rate, exposure time, pH and conductivity on bacterial inactivation performance were investigated to understand correlations among these parameters. It was found that inactivation efficiency up to 98% was obtained under -6.6 kV voltage, 2 cm distance between needle tip and counter electrode, pH=7, 0.20 mS/cm of conductivity, 25 min of exposure time and 2 μL/min of flow rate. Results indicate that the electrospray technology is a potentially chemical-free alternative to conventional methods (e.g., chlorine spraying) in decontaminating surfaces of livestock buildings.

5.2 Introduction

Microbial contamination has the potential to impact the health of livestock and workers in animal confinement facilities [1, 2]. Bacteria found in livestock may infect humans. *E.coli* for instance, was found to cause approximately 20,000 infections and 200 human deaths each year in the United Sates [3]. Therefore, more efforts should be made to improve farm worker's and livestock's health, and to minimize disease transmission to human.

Some of the current disinfection methods used in livestock facilities include hydrogen peroxide [4], chlorine [4], and Ultraviolet irradiation [5]. Their advantages and disadvantages

are presented in Table 5.1.

Table 5.1 Current disinfectants used in livestock facilities.

	Advantages	Drawbacks
Hydrogen peroxide[a]	• Highly oxidative	• Leaves chemical residuals
Chlorine[a]	• Highly oxidative	• Leaves chemical residuals • Odor objections
Ultraviolet irradiation[b]	• Very effective in killing all kinds of microorganisms, especially drug resistant bacteria	• UV light can damage human skin and eyes • UV light can cause damage to plastics and rubber materials

[a]Source: Campagna et al. [4].

[b]Source: Cossu et al. [5].

More recently, a novel and chemical free nanotechnology-based method has been reported for foodborne bacteria inactivation. It has been found to reduce bacteria up to 2.5 log [6]. In this technique, an electrospray system generates nano scaled engineered water droplets (EWNS) that contains reactive oxygen species (ROS) that can deactivate bacteria [7]. EWNS droplets that carry ROS can kill bacteria by damaging membrane structures. The nano scaled water droplets have an electron rich water shell that can change its mobility and lifetime dramatically from milliseconds to minutes [8].

This EWNS technology has been tested in inactivating *E.coli* inoculated on tomato and

blackberry surfaces [6, 9]. The results have shown that EWNS can achieve about 1 log reduction on tomato surface and 1.2 log reduction on blackberry surface after exposing them to EWNS droplets for 90 min. However, there is no research conducted to evaluate the performance of EWNS technology on inactivating bacteria in livestock facilities.

The current study aimed to investigate the inactivation efficacy of bacteria collected from a poultry barn using the EWNS method by varying operating parameters such as voltage level and polarity, distance between needle tip and counter electrode, liquid flow rate, conductivity, EWNS exposure time, and pH. The inactivation efficacies under those parameters were evaluated by using LB agar plates to collect bacteria from poultry barn.

5.3 Methods and materials

5.3.1 Mechanisms for the generation of engineered water nanostructures (EWNS)

The mechanism of generating EWNS is the same as previously discussed in Chapter 4. In general, there are two mechanisms associated with the generation of EWNS, namely, electrospray and ionization. As shown in Figure 4.1 in Chapter 4, a high voltage current (usually in the range of kilovolts) is applied to a metal capillary, which then charges the water passing through it. The strong electric field developed between the metal capillary and counter electrode causes the formation of a so-called Taylor cone at the outlet of the capillary [6]. As the highly charged water droplets at the tip of the Taylor cone are drawn to the counter electrode by electric force, they continue to break into smaller droplets in a size ranging from millimeters to nanometers. According to Pyrgiotakis et al. [8], a typical nano-size water droplet normally disappears within milliseconds due to evaporation. However, the electric charges present within the water droplets could significantly increase the surface tension and reduce the

evaporation rate of the water droplets, thereby increasing their lifetime [10]. Depending on the operating conditions employed during production of EWNS aerosols, the droplet size distribution can have a diverse histogram, including monodisperse and polydisperse [6]. During the electrospray and ionization process, the high electric field causes some water molecules and air molecules (O_2) to split and lose electrons, resulting in the formation of ROS [8].

5.3.2 Experimental setup

The experimental setup is the same as previously discussed in Chapter 4. The experiments were conducted inside a Plexiglass chamber (35 cm x 35 cm x 35 cm). As shown in Figure 5.1, a syringe pump (NE-1000, New Era Pump Systems Inc., Farmingdale, USA), mounted on the top of the chamber, was used to control the liquid flow rate. In Chapter 3, it was shown that the minimum flow rate for water in order to establish a steady cone-jet formation equaled 0.55 µL/min. Hence, the flow rates evaluated in this paper were 1, 2 and 4 µL/min. The liquids used in this study were RO water, deionized water, saline water, and caustic solutions. The caustic solutions with pH=8.5 and 10 were prepared by adding sodium hydroxide into the RO water. Saline water (NaCl solution) with K=14.72 mS/cm was purchased from Fisher Scientific, Canada. The liquid was placed in a 2.5 mL syringe (1000 series Gas Tight, Hamilton, USA), which was coupled with a 30 Gauge needle (Metal Hub, Fisher Scientific, USA) with an inner diameter of 0.159 mm and an outer diameter of 0.311 mm. The electrical conductivities and pH values of the liquids were measured using a conductivity meter (Omega PHH-7200, ALPHAOMEGA Electronics, Spain) and a pH meter (Omega PHH-7200, ALPHAOMEGA Electronics, Spain). The temperature and relative humidity inside the chamber were

continuously monitored using a temperature and relative humidity probe (HIH8120-021-001, Humidlcon, Honeywell, USA). The ozone was measured by using a digital ozone sensor (DGS-O3 968-042, SPEC Sensor, USA) with an accuracy of ± 15%.

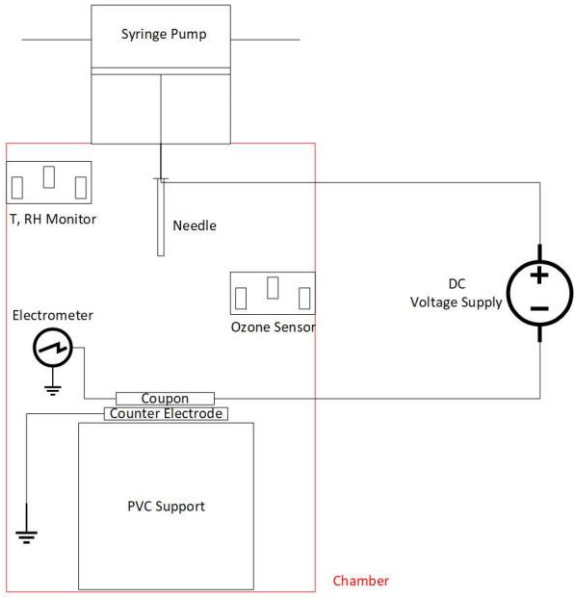

Figure 5.1 Schematic of the experiment setup.

As shown in Figure 5.1, right below the syringe needle was a 5 cm diameter stainless-steel coupon. The coupon was placed on top of a grounded counter electrode (5.85 cm in diameter and 0.1 cm thick), which was made of alumina. Beneath the counter electrode was an adjustable polyvinyl chloride (PVC) support used to change the distance (i.e., 2, 3 and 4 cm) between the tip of the needle and the counter electrode. The electric field within the system was generated by connecting the needle to a high voltage power supply (APM-30KIPNX, Kasuga Denkie Inc., Japan), which supplied the system voltage levels from -10 to +10 kV, and the counter electrode to the ground port of the power supply.

5.3.3 Poultry barn bacteria collection, preparation and cfu counting

Six identical LB (DF0446-17-3, Fisher Scientific, Canada) agar plates were placed in the same poultry room for a period of 5 min, exposing the LB agar to the air in the barn to collect bacteria, including airborne bacteria and poultry dust. Then, all the agar plates were properly sealed and brought back to the lab. Three of the agar plates were used as controlled samples and the other three of the agar plates were used for EWNS treatment. Each agar plate was cut into a rectangle with an area of 1.5 cm x 1.5 cm, which is sufficiently large enough to cover the electrosprayed area based on the result from Chapter 3. Once preparation of the agar plates was completed, the EWNS treatment plates was directly placed under the electrospray with the bacteria side facing the needle tip. The exposure time and all the other operating conditions employed in the study are listed in Table 5.2. The operating ranges and baselines were selected and set based on the hypothesis presented in Chapter 1 and V-I characteristic curves shown in Chapter 3. Each operating condition was performed in triplicates to ensure the accuracy of the results. All experiments were conducted at a constant temperature of 20 ℃ and relative humidity of 25%. After the electrospray was finished, the EWNS treatment agar plate was placed in an incubator (650D, Fisher Scientific, Canada) and incubated for 8 hours at 37℃ prior to colony counting.

Table 5.2 Operating conditions employed in the poultry barn bacteria deactivation experiments.

Operating condition	Voltage (kV)	Distance between needle tip and counter electrode (cm)	Exposure time (min)	Flow rate (µL/min)	Conductivity (mS/cm)	pH
1 (Baseline)	-6.6	3	25	2	0.20	7
2	-7.6	3	25	2	0.20	7
3	6.6	3	25	2	0.20	7
4	-6.6	2	25	2	0.20	7
5	-6.6	4	25	2	0.20	7
6	-6.6	3	15	2	0.20	7
7	-6.6	3	35	2	0.20	7
8	-6.6	3	25	1	0.20	7
9	-6.6	3	25	4	0.20	7
10	-6.6	3	25	2	0.06	7
11	-6.6	3	25	2	14.72	7
12	-6.6	3	25	2	0.20	8.5
13	-6.6	3	25	2	0.20	10

5.3.4 Data analysis

The inactivation efficiency of EWNS produced by the electrospray was estimated through Equation 5.1 for each treatment condition. A standard deviation of means was used to represent the error bar.

$$Bacteria\ Deactivation\ Efficiency = 1 - \left(\frac{\frac{CFU\ in\ the\ effective\ area}{Effective\ area}}{\frac{CFU\ in\ the\ controlled\ area}{controlled\ area}}\right) \quad (5.1)$$

where,

The effective area is the area directly exposed to the electrospray.

The controlled area is the area in the controlled agar plate ≈ (1.5 cm x 1.5 cm).

5.4 Results and discussion

5.4.1 The effect of ozone on bacteria deactivation efficiency

In the electrospray process, water molecules and air molecules (O_2) can split and lose electrons due to an electric field that causes the generation of ozone along with ions and ROS [8]. As mentioned in the literature review section, ozone is a strong oxidative chemical agent and its antimicrobial activity have been studied extensively and proved to be effective against many strains of bacteria [11]. In order to examine the contribution of the ozone to microbial deactivation under negative voltage polarity, two of the rectangle agar plates were placed on the stainless-steel coupon, where the first plate was directly placed under the electrospray and the other plate was placed on the side of the coupon (illustrated in Figure 5.2). This experiment was performed in triplicates. Since the system was in a closed chamber, the plate on the side was able to indicate whether the ozone had an effect on bacteria deactivation. In Figure 5.3, the picture on the right-hand side showed that the ozone had negligible effect on bacteria deactivation, because the number of colony forming unit (cfu) for the ozone treatment about almost equaled to the number of cfu for the controlled sample. Pyrgiotakis et al. [8] had also demonstrated in their work that ozone level and the exposure time had zero impact on the bacteria inactivation results. The ozone sensor detected an average of 113 ppb of ozone presented in the chamber.

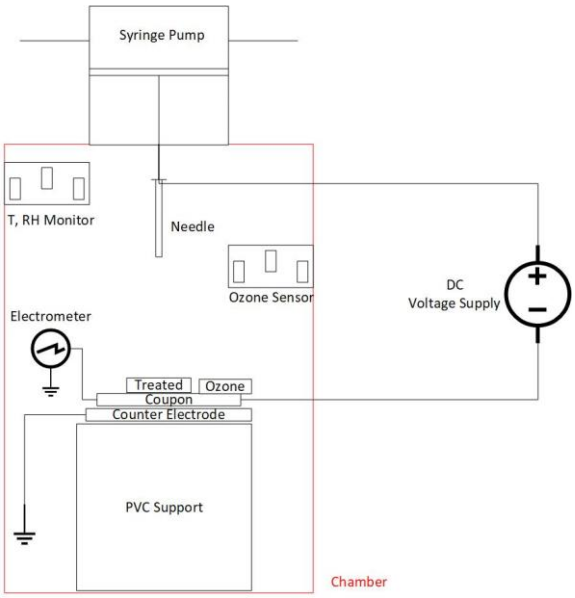

Figure 5.2 Elimination of the ozone effect – setup.

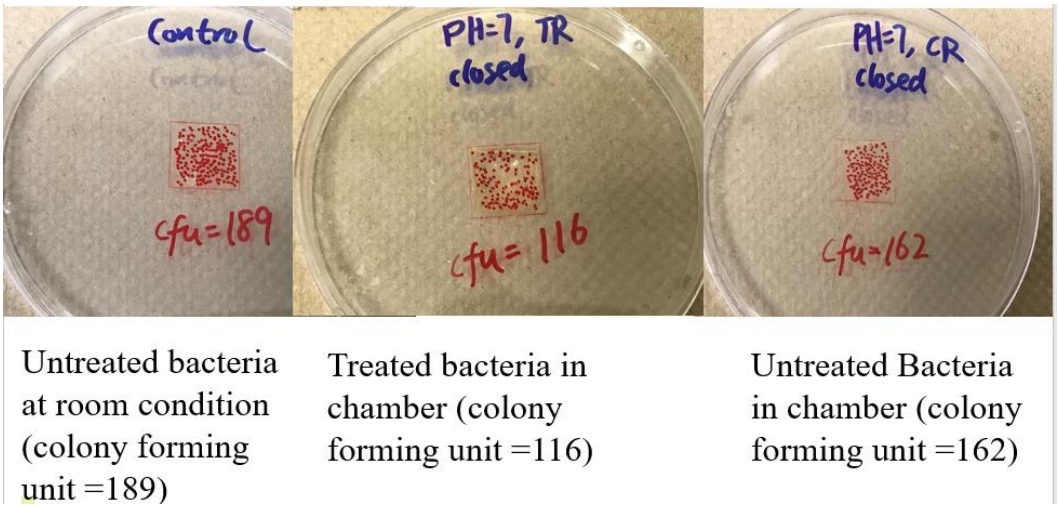

Figure 5.3 Comparison of different samples under different treatments.

5.4.2 Poultry barn bacteria deactivation efficiency at various operating conditions

5.4.2.1 The effect of voltage level and polarity on bacteria deactivation efficiency

As described in Chapter 4, a sensitivity test was established and conducted by changing one operating parameter at a time while the others were kept constant. Figure 5.4 shows the poultry barn bacteria deactivation efficiency obtained from altering the applied voltage only. With an increase in the negative voltage from -6.6 to -7.6 kV, the bacteria deactivation efficiency increased from 88% to 94%. A similar result was obtained from the *E.coli*

experiment, where more ROS generated at a higher voltage. By comparing -6.6 against +6.6 kV, the negative voltage demonstrated a higher bacteria deactivation efficiency with 88% compared to 83% for the positive voltage polarity. A similar result was obtained from the *E.coli* trial, where negative voltage facilitated a greater mobility of negative charges [12].

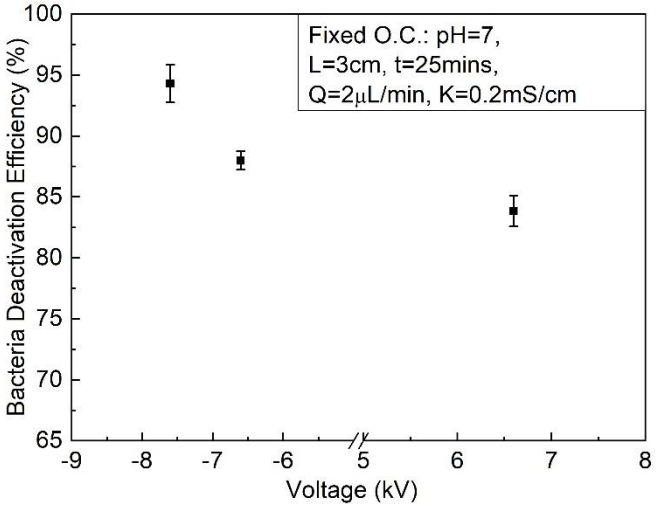

Figure 5.4 Effect of voltage level and polarity on poultry barn bacteria deactivation efficacy. This employed operating conditions: 1, 2 and 3 (From Table 5.2). Fixed O.C. is "fixed operating condition".

5.4.2.2 The effect of distance on bacteria deactivation efficiency

Figure 5.5 shows the result of poultry barn bacteria deactivation efficiency when the distance between the needle tip and counter electrode was changed while other operating parameters were kept the same. This employed operating conditions of 1, 4 and 5, corresponded to 3, 2 and 4 cm distances, respectively. When the distance was 2 cm, the highest antibacterial efficiency of about 98% was obtained at exposure duration of 25 min. Increasing the distance from 2 cm to 4 cm had an adverse effect on the bacteria deactivation efficiency. The efficiency dropped from 98% to approximately 73% due to an increase in the distance. Similar result was obtained from the *E.coli* experiment at the same operating condition and this phenomena can

be explained in Equation (4.3) in Chapter 4.

A shorter distance between the needle tip and counter electrode results in a higher current and more electric charges (explained in Chapter 3), thus producing more ROS.

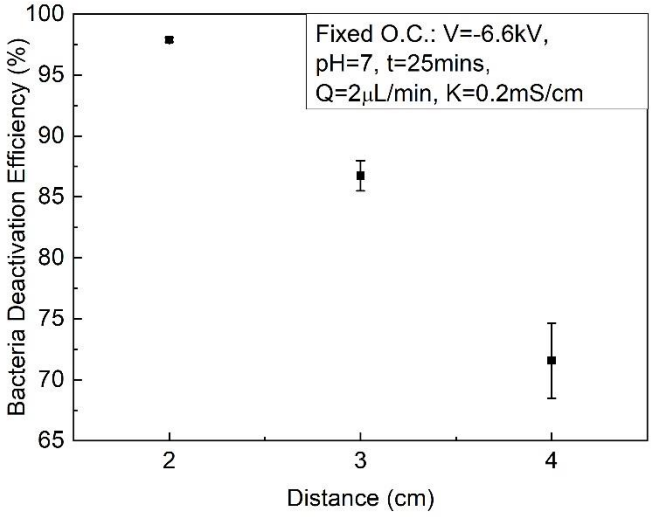

Figure 5.5 Effect of needle tip to counter electrode distance on poultry barn bacteria deactivation efficacy. This employed operating conditions: 1, 4 and 5 (From Table 5.2).

5.4.2.3 The effect of EWNS exposure time on bacteria deactivation efficiency

It can be seen in Figure 5.6 that the poultry barn bacteria deactivation efficiency increased from 72% to 92% with an increase of the EWNS exposure time from 15 to 35 min. Both the *E.coli* trial and Vaze et al. [6] obtained the same results. With a longer EWNS exposure time, the bacteria would experience more protein and DNA damage [6].

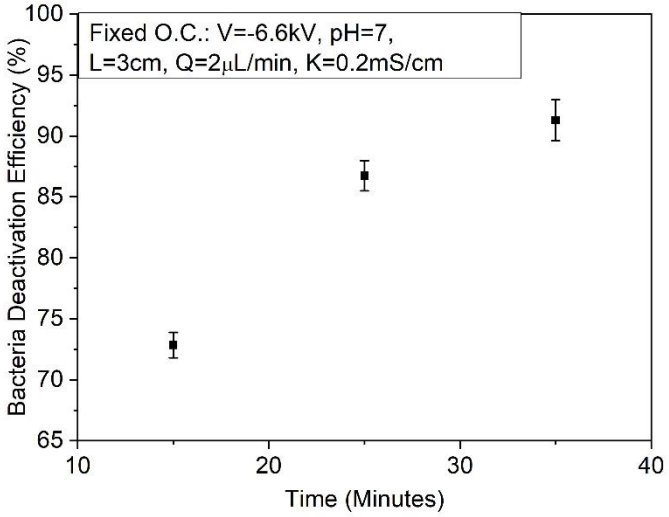

Figure 5.6 Effect of EWNS exposure time on poultry barn bacteria deactivation efficacy. This employed operating conditions: 1, 6 and 7 (From Table 5.2).

5.4.2.4 The effect of liquid flow rate on bacteria deactivation efficiency

The liquid flow rate contributes significantly to the performance of EWNS in deactivating poultry barn bacteria. As shown in Figure 5.7 below, with the liquid flow rate increased from 1 to 2 μL/min, the corresponding efficiency increased from 76% to 86%. This is not observed in the *E.coli* trial because the poultry barn bacteria not only includes *E.coli*, but also includes other strains of bacteria and poultry dust, which might affect the deactivation efficiency of EWNS. When the liquid flow rate changed from 2 to 4 μL/min, the deactivation efficiency dropped from 86% to 70%. A similar trend was observed in the *E.coli* trials discussed in Chapter 4.

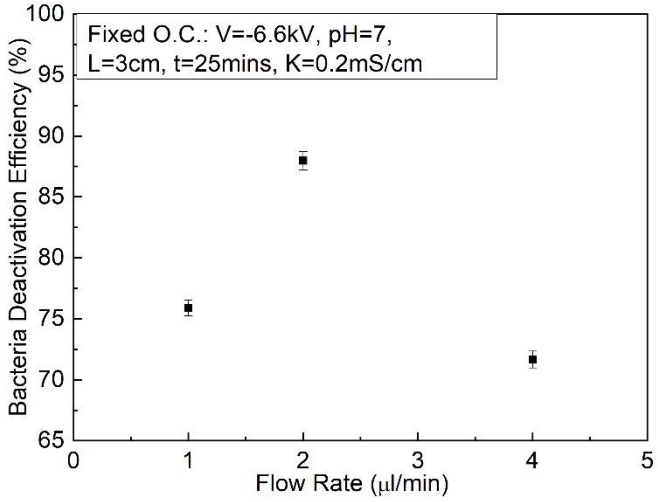

Figure 5.7 Effect of liquid flow rate on poultry barn bacteria deactivation efficacy. This employed operating conditions: 1, 8 and 9 (From Table 5.2).

5.4.2.5 The effect of pH and conductivity on bacteria deactivation efficiency

Figure 5.8 indicates that the poultry barn bacteria deactivation efficiency was the highest, 92%, when pH reached 10 compared to pH=7 and 8.5, which had efficiencies of 88% and 89%, respectively. This is consistent with the *E.coli* trial result, showing that more bacteria is deactivated when increasing the pH from neutral to caustic. As shown in Figure 5.9, mili-Q water (K=0.06 mS/cm) had the lowest bacteria deactivation efficiency of 86%, then came RO water (K=0.20 mS/cm), which had an efficiency of 88%. Medically used saline water (K=14.72 mS/cm) had the highest bacteria deactivation efficiency, which was 93%. The same result was obtained in the *E.coli* trial: higher liquid conductivity may result in higher bacteria inactivation rate.

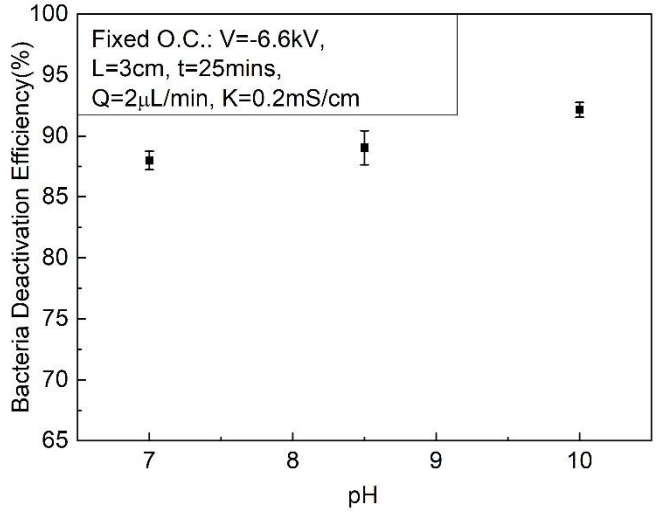

Figure 5.8 Effect of liquid pH on poultry barn bacteria deactivation efficacy. This employed operating conditions: 1, 10 and 11 (From Table 5.2).

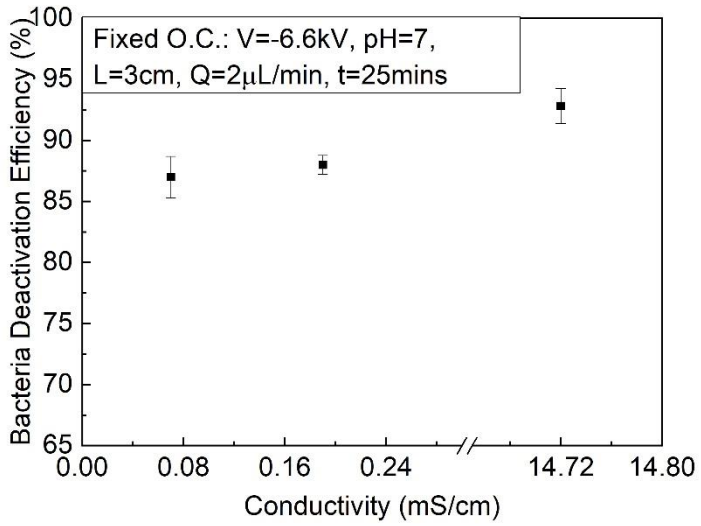

Figure 5.9 Effect of liquid conductivity on poultry barn bacteria deactivation efficacy. This employed operating conditions: 1, 12 and 13 (From Table 5.2).

5.5 Conclusions

In this work, the effects of applied voltage level and polarity, distance between needle tip and counter electrode, EWNS exposure time, liquid flow rate, pH and conductivity on poultry barn bacteria inactivation rates were investigated.

It was found that higher voltage (-7.6 kV), shorter distance between needle tip and counter electrode (2 cm), longer exposure time (35 min), lower flow rate (2 µL/min), higher pH (10) and conductivity (14.72 mS/cm) resulted in higher poultry barn bacteria deactivation efficiency. This work also demonstrated that EWNS could potentially be used as an effective decontamination method in livestock barns.

5.6 Acknowledgements

Support from the University of Saskatchewan, Agriculture Development Fund (ADF) from the Ministry of Agriculture of Saskatchewan, and Agrivita Canada Inc. is greatly appreciated.

5.7 References

[1] Kirychuk, S., Just, N., Gilbert, Y., Letourneau, V., Veillette, M., Singh, B., Duchaine, C., 2011. Bacterial diversity characterization of bioaerosols from cage-housed and floor-housed poultry operations. *Environmental Research*, vol. 111, pp. 492-98.

[2] Predicala BZ, Maghirang RG, Jerez SB, Urban JE, Goodband RD., 2001. Dust and bioaerosol concentrations in two swine-finishing buildings in Kansas. *American Society of Agricultural Engineers*, vol. 44, pp. 1291-98.

[3] Todd R, C., MA, C., TS, E., Robin C, A., & David J, N., 2009. Diet, Escherichia coliO157:H7, and Cattle: A Review After 10 Years. *Current Issues in Molecular Biology*, 6, pp.31-42. doi: 10.21775/cimb.011.067

[4] Campagna, M. V., Faure-Kumar, E., Treger, J. A., Cushman, J. D., Grogan, T. R., Kasahara, N., & Lawson, G. W., 2016. Factors in the Selection of Surface Disinfectants for Use in a Laboratory Animal Setting. *Journal of the American Association for Laboratory Animal*

Science: JAALAS, 55(2), pp.175–188.

[5] Cossu, A., Huang, K., Cossu, M., Tikekar, R., & Nitin, N., 2018. Fog, phenolic acids and UV-A light irradiation: A new antimicrobial treatment for decontamination of fresh produce. *Food Microbiology*, 76, pp.204-208. doi: 10.1016/j.fm.2018.05.013

[6] Vaze, N., Jiang, Y., Mena, L., Zhang, Y., Bello, D., Leonard, S., Morris, A., Eleftheriadou, M., Pyrgiotakis, G. and Demokritou, P., 2018. An integrated electrolysis – electrospray – ionization antimicrobial platform using Engineered Water Nanostructures (EWNS) for food safety applications. *Food Control*, 85, pp.151-160.

[7] Pyrgiotakis, G., McDevitt, J., Bordini, A., Diaz, E., Molina, R., Watson, C., Deloid, G., Mizuyama, Y., Brain, J., Demokritou, P., 2014. A chemical free, nanotechnology-based method for airborne bacterial inactivation using engineered water nanostructures. *Environ Sci Nano*, pp. 15-26.

[8] Pyrgiotakis, G., McDevitt, J., Yamauchi, T. and Demokritou, P., 2012. A novel method for bacterial inactivation using electrosprayed water nanostructures. *Journal of Nanoparticle Research*, 14(8), pp.1027-1038.

[9] Pyrgiotakis, G., Vasanthakumar, A., Gao, Y., Eleftheriadou, M., Toledo, E., DeAraujo, A., McDevitt, J., Han, T., Mainelis, G., Mitchell, R. and Demokritou, P., 2015. Inactivation of Foodborne Microorganisms Using Engineered Water Nanostructures (EWNS). *Environmental Science & Technology*, 49(6), pp.3737-3745.

[10] Nielsen, J., Maus, C., Rzesanke, D. and Leisner, T., 2011. Charge induced stability of water droplets in subsaturated environment. *Atmospheric Chemistry and Physics*, 11(5), pp.2031-2037.

[11] Muhlisin, M., Utama, D., Lee, J., Choi, J. and Lee, S., 2016. Effects of Gaseous Ozone Exposure on Bacterial Counts and Oxidative Properties in Chicken and Duck Breast Meat. *Korean Journal for Food Science of Animal Resources*, 36(3), pp.405-411.

[12] English, W., 1948. Corona from a Water Drop. *Physical Review*, 74(2), pp.179-189.

Chapter 6 – Conclusions and recommendations

6.1 Summary of results

The electrical current was first investigated in an electrospray system by measuring the current from the stainless-steel coupon. The operating conditions include voltage level and polarity, needle tip to counter electrode distance, liquid flow rate, pH and conductivity. By increasing the positive voltage to +10 kV, the electrical current increased from 3.5 µA at 4 cm distance to 12.2 µA at 2 cm distance. The liquid flow rate did not show an impact on the electrical current measured within the range investigated in this work. The electrical current increased from 5.8 µA to 6.3 µA when pH increased from 7 to 9.76. The electrical current increased from 5.8 µA to 6.2 µA when conductivity increased from 0.20 mS/cm to 13.94 mS/cm. A similar result was obtained for negative voltage.

The size of EWNS was measured by AFM under an operating condition of 3 cm distance, 4 µL/min liquid flow rate and -6.6 kV voltage. It was found that EWNS droplets were produced with a mean diameter of 299 nm, a mode of 316 nm and a standard deviation of 76 nm (geometric standard deviation 1.29).

The electrosprayed area was considered to be one of the most important factors that would assist us to scale up the electrospray system. A larger electrosprayed area was observed for negative voltage (23.1 mm^2) compared to positive voltage (16.7 mm^2) because a greater electrostatic force was experienced in the system. With an increase in the liquid flow rate, distance between the needle tip and the counter electrode, pH and conductivity, the electrosprayed area increased from 19.8 mm^2 at 1 µL/min to 68.9 mm^2 at 5 µL/min; and increased from 20.2 mm^2 at 2 cm distance to 23.1 mm^2 at 3 cm distance; and increased from

23.1 mm^2 at pH=7 to 32.6 mm^2 at pH=10 and increased from 23.1 mm^2 at 0.20 mS/cm to 35.4 mm^2 at 13.94 mS/cm.

E.coli and poultry barn bacteria deactivation efficiency undergoes the same trend when altering operating parameters. More specifically, the *E.coli* deactivation increased from 2.43 log to 2.95 log when the applied voltage increased from -6.6 to -7.6 kV; while the poultry barn bacteria deactivation efficiency increased from 88% to 94% under the same condition. The EWNS exposure time, liquid pH and conductivity increased with an increase of *E.coli* and poultry barn bacteria inactivation rate. The main contributing factors that result in a higher inactivation efficacy are summarized as follows.

1. Longer EWNS exposure time to the bacteria.
2. More hydroxyl radicals presented in caustic solution.
3. Higher electrical current and charges.

An increased liquid flow rate and distance between the needle tip and the counter electrode led to decreased *E.coli* and poultry barn bacteria inactivation rates because of shorter contact time between fluid and electrode and lower electrical current.

6.2 Conclusions

(1). EWNS generated the highest microbial deactivation efficiency compared to non-thermal plasma and empty needle.

(2). It was found that higher the voltage of the power supply, higher the pH and conductivity of the solution, higher the bacteria deactivation efficiency.

(3). It was found that the highest *E.coli* inactivation rate was reached when the system experienced -7.6 kV voltage, 2 cm distance between needle tip and counter electrode, 1 μL/min of flow rate, 45 min of exposure time, 14.72 mS/cm of conductivity and pH=12.

(4). It was found that the highest poultry barn bacteria inactivation rate was reached when the system experienced -7.6 kV voltage, 2 cm distance between needle tip and counter electrode, 2 μL/min of flow rate, 35 min of exposure time, 14.72 mS/cm of conductivity and pH=10.

6.3 Recommendations

In this study, *E.coli* was an appropriate model for determining the bacteria deactivation efficiency since it is a common gram-negative bacteria found in livestock barns. In actual conditions, there are many other types of bacteria in livestock barns, including gram-negative and gram-positive bacteria. Gram-positive bacteria have thicker layers of cell walls compared to that of gram-negative bacteria. The deactivation efficiency of gram-positive bacteria has not been examined. Therefore, the effect of all the above-mentioned operating conditions on the performance of EWNS deactivating gram-positive bacteria (staphylococcus) should be investigated in future work.

For the poultry barn bacteria deactivation trial, a similar recommendation is provided to collect bacteria from different livestock barns (Ex. swine barn) to investigate different operating conditions on the performance of EWNS inactivating harmful microbes.

In this work, the bacteria collected in the poultry barn were not specified. In the near future, a DNA sequencing could be done to determine and identify the bacteria in poultry barn to better understand the performance of EWNS on each bacterium.

The EWNS droplet size was tested and measured under only one operating condition, so more work and effort in this area should be done to further investigate different operating conditions on the size of EWNS droplets.

Overall, EWNS is an effective bacteria deactivation technology that could be applied in livestock facilities.

Appendix A – Experiment setup

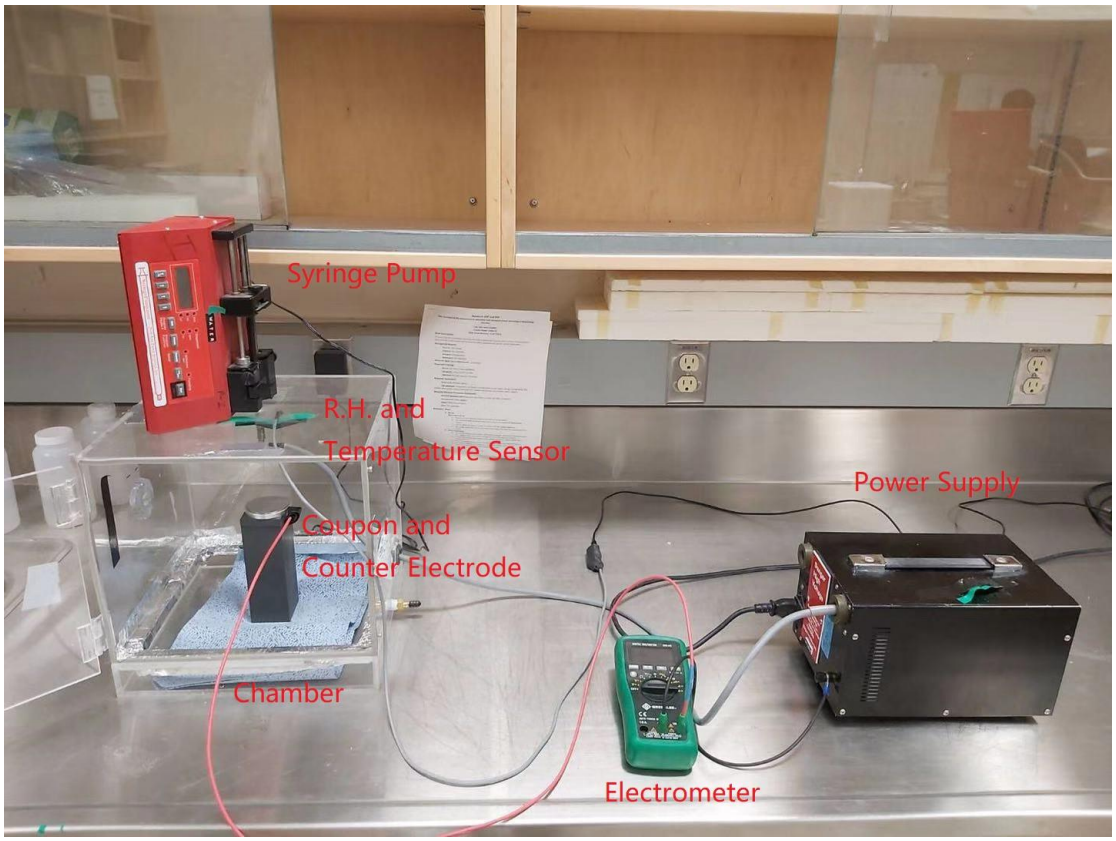

Figure A.1 Experiment setup.

Appendix B – Electrospray with stainless-steel coupon and needle tip

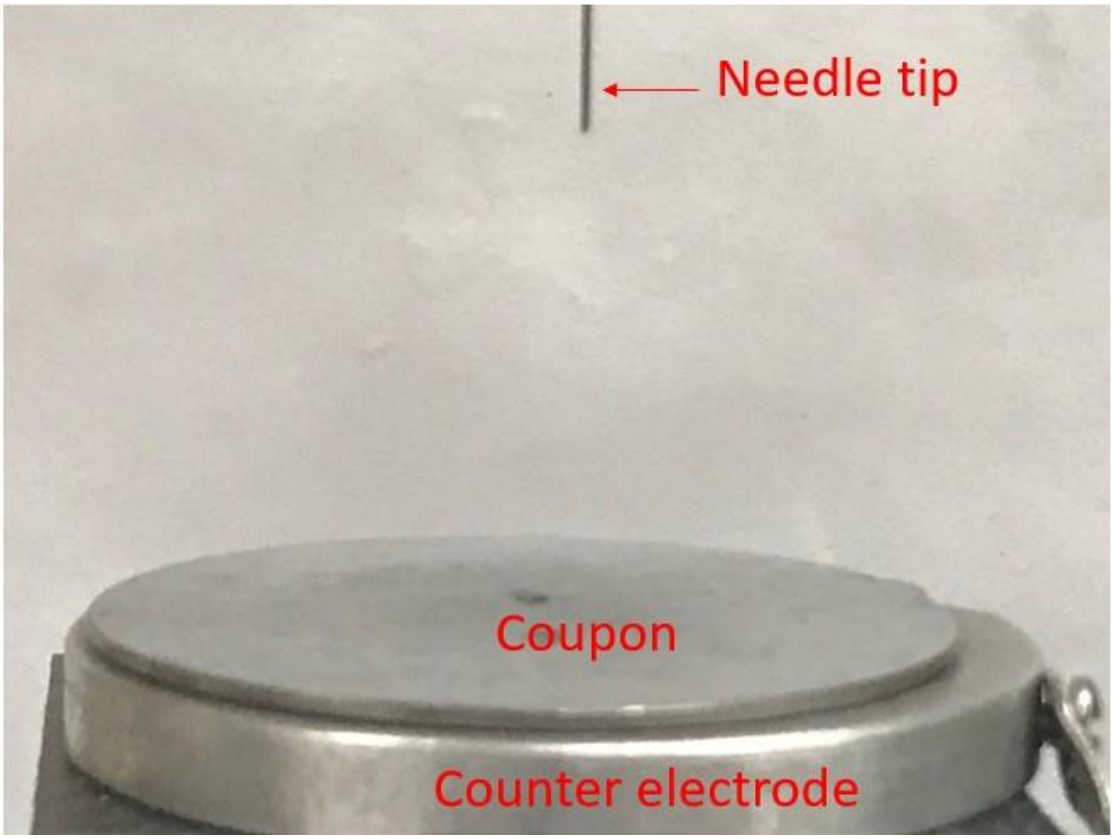

Figure B.1 Electrospray with stainless-steel coupon and needle tip

Appendix C – Procedures for preparing *E.coli*

C.1) Preparation of LB broth

a. Weigh out 12.5g of LB Broth powder (BD Difco, Fisher Scientific, Cat#DF0446-17-3) using a top loading balance and place into a 1L Nalgene bottle.
b. Dissolve the LB broth powder in 500 mL of distilled water.
c. Unscrew the lid to the bottle so it is loose, cover the lid with tin foil and put a piece of autoclave tape with: media type, date, lab #, and initials/PI's initials. Put the bottles of media in a solid container and place on the cart for autoclaving.

C.2) Preparation of LB Agar plates

a. Weigh out 7.5 g of granulated Agar (BD Difco, Fisher Scientific) and 12.5g of LB broth powder using a top loading balance. Place both into a 1L Nalgene bottle.
b. Dissolve the powder in 500 mL of distilled water.
c. Unscrew the lid to the bottle so it is loose, cover the lid with tin foil and put a piece of autoclave tape with: media type, date, lab #, and initials/PI's initials. Put the bottles of media in a solid container and place on the cart for autoclaving.
d. Cool the agar down in a 65°C water bath.
e. In the biosafety cabinet, pour agar into petri plates covering approximately $\frac{3}{4}$ of the plate. Close the lids to the plates and swirl gently to distribute the agar across the petri plate.
f. Allow the plates to solidify. Store at 4°C if not using right away.

C.3) Preparation of *E. coli* after receiving from supplier

a. In the biosafety cabinet, open the vial according to the manufacturer's instructions.
b. Add 0.5 to 1 mL of LB broth to the tube containing the pellet using a pipette.
c. Mix contents of the tube by pipetting up and down gently.
d. Aseptically transfer this aliquot to a tube containing LB Broth (5 to 6 mL) and mix well.
e. Using a sterile disposable loop, streak the culture onto LB agar plates.
f. Incubate the tube and plates at 37°C for 16-18 hours.

C.4) *E. coli* inoculation (plate to plate)

a. Use sterile disposable loop to attach one single colony of *E. coli* from original agar plate.
b. Close the original petri dish.
c. Partially lift the lid of the petri dish containing the solid LB-A medium.
d. Hold the charged loop parallel with the surface of the agar, smear the inoculum backwards and forwards across a small area of the medium (see streaked area A in photograph).
e. Turn the dish 90° anticlockwise, with the same loop streak the plate from area A across the surface of the agar in three or four parallel lines (B). Make sure that a small amount of culture is carried over.
f. Turn the dish 90° anticlockwise again and streak from B across the surface of agar in three or four parallel lines (C).
g. Turn the dish 90° anticlockwise and streak loop across the surface of agar from C into the centre of the plate (D).
h. Remove and dispose the loop, close the Petri dish.
i. Seal and store at 4° for maximum two weeks.

(All procedures of inoculation above are performed in the biosafety cabinet.)

C.5) *E. coli* inoculation (plate to liquid culture medium):

a. Use sterile disposable loop to attach one single colony of *E. coli* from agar plate.
b. Close the Petri dish.
c. Dip the loop inside a 10 ml Falcon tube containing 5 ml of liquid LB medium and mix slowly.
d. Close the Falcon tube and dispose the loop.
e. Incubate the culture medium at 37 °C for 12 to 20 hours.

(All procedures of inoculation above are performed in the biosafety cabinet.)

C.6) Optical density determination

a. Take 1 mL of culture and put it into a plastic cuvette.
b. Recap the Falcon tube with liquid culture medium.

c. Wipe down the outside of the cuvette with a kimwipe to remove any thing that could interfere with the OD reading.
d. Use the single wavelength mode of UV-Vis spectrophotometer to measure the absorbance of 1 ml incubated LB medium at 600 nm (LB culture as blank).
e. If the OD>1, the sample dilution is needed.

(The OD reading can be performed on the bench)

C.7) Characterize the deactivation efficiency

a. 10 µL of the pre-determined concentration of *E. coli* stock solution will be withdrawn and dipped onto the center of a stainless-steel coupon (Autoclaved).
b. Recap the stock solution and place the coupon in a petri dish with lid on.
c. The inoculated coupon is allowed to dry for 10 min in biosafety cabinet before transferring the coupon to the chamber.
d. After 10 min of drying, *E.coli* is recovered from the coupon following steps e to g and this concentration is set as *E.coli* concentration at t=0.
e. The inoculated *E.coli* will be treated under the electrospray for 15, 25, 45 min to deactivate the bacteria.
f. After the treatment, the coupon is washed by 1 mL of autoclaved water to recover *E.coli* and transfer the solution to Eppendorf tube.
g. 100 µL of the solution is then withdrawn from the Eppendorf tube and plated on the LB agar plate.
h. Steps a to f is repeated in triplicates.
i. Seal the plates with parafilm and incubate at 37 °C for 16-18 hours.
j. If number of colonies are too numerous to count on the plates, then less *E. coli* solution needs to be used for inoculation.

(All procedures of inoculation above are performed in the biosafety cabinet.)

Appendix D – Natural decay on *E.coli*

In order to take natural decay of the bacteria into consideration, the stainless-steel coupon with *E.coli* inoculated on the surface was placed inside the petri dish. Then, the petri dish was sealed properly and left in the biosafety cabinet for a period of 15, 25 and 45 min. As shown in Figure D.1 below, natural decay contributed roughly 0.17 log at 15 min, 0.22 log at 25 min and 0.38 log at 45 min. All the results were calculated according to Equation 4.1 in Chapter 4. By comparing with the baseline condition (Table 4.1 in Chapter 4), the average contribution of natural decay on *E.coli* deactivation efficiency was approximately 11% when considering all three time intervals. Therefore, natural decay of *E.coli* did not have a significant impact ($p>0.05$) on the bacteria deactivation efficiency (log reduction).

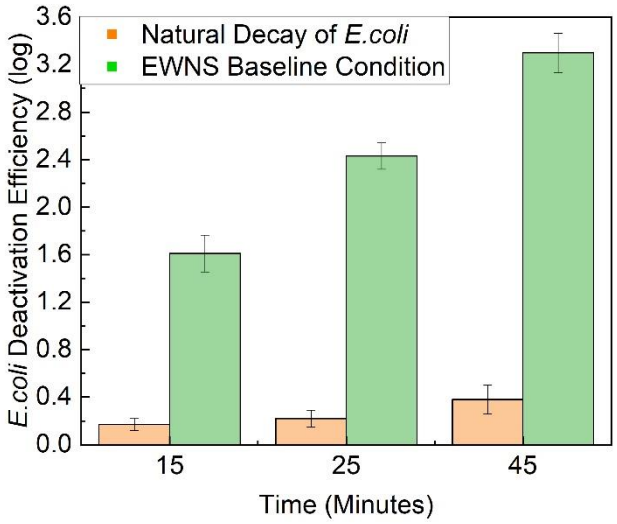

Figure D.1 Comparison between natural decay and EWNS deactivation efficiency at baseline condition (Table 4.1) on *E.coli*.

Appendix E – Effect of ozone on *E.coli*

The experiment schematic is shown in Figure E.1 and the procedures of the experiment are the same as those shown in Chapter 4 except another inoculated *E.coli* coupon was placed at the same height beside the electrosprayed sample to test whether ozone impacted *E.coli* deactivation efficiency. It was clearly demonstrated in Figure E.2 that the *E.coli* deactivation efficiency was approximately 0.28 log (including 0.24 log of natural decay) under the influence of ozone (O_3 average concentration = 151 ppb) for a period of 25 min. This result showed that ozone had negligible impact ($p>0.05$) on the bacteria deactivation efficiency. Pyrgiotakis et al. [1] had also demonstrated in their work that ozone level and the exposure time had minimal impact on the bacteria inactivation results.

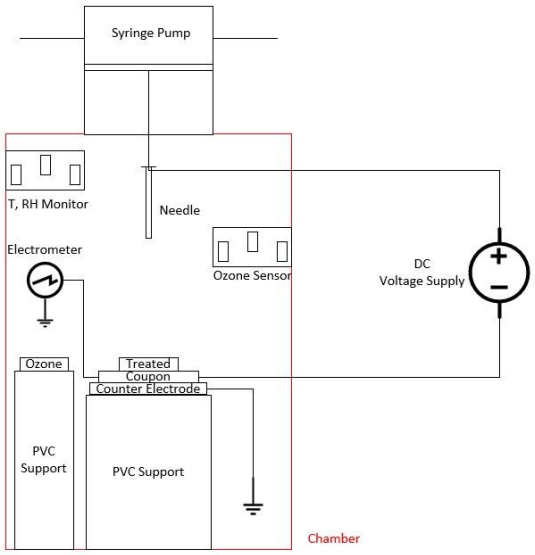

Figure E.1 Experiment schematic for *E.coli* ozone test.

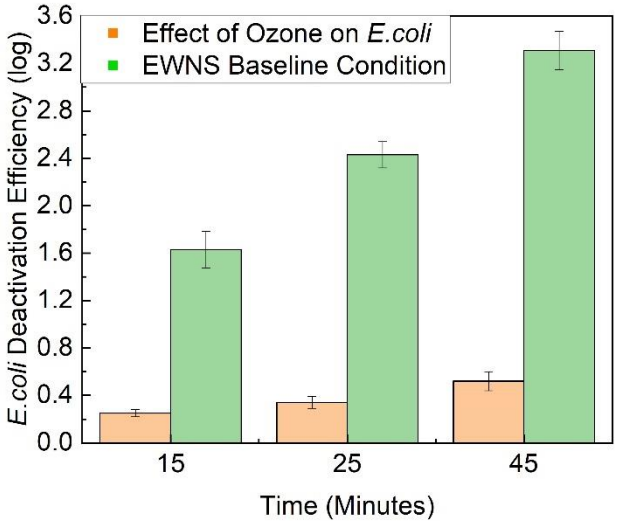

Figure E.2 Comparison between ozone and EWNS deactivation efficiency at baseline condition (Table 4.1) on *E.coli*.

E.1 References

[1] Pyrgiotakis, G., McDevitt, J., Yamauchi, T. and Demokritou, P., 2012. A novel method for bacterial inactivation using electrosprayed water nanostructures. Journal of Nanoparticle Research, 14(8), pp.1027-1038.

Appendix F – Effect of EWNS and ozone on agar nutrient

Swine barn bacteria was collected using a similar method as discussed previously in Chapter 5. However, the objective of this swine barn experiment was to investigate whether the charged droplets and ozone could cause irreversible damage on Lysogeny broth (LB) (DF0446-17-3, Fisher Scientific, Canada) agar nutrient. Therefore, in this work, LB agar plates were first exposed to electrospray and then ozone for a period of 25 min. Secondly, these agar plates and unexposed plates (controlled samples and field blanks) were placed directly under the swine barn ventilation fan (exhaust) for 2 min. Then, all the agar plates were properly sealed and stored in the Styrofoam ice box before placing them in the incubator at 37 ℃ for 22 hours. As shown in Figures F.1 and F.2 below, the controlled samples roughly had the same number of colony forming units (cfu) as compared to the treated samples (exposed to electrospray and ozone). Hence, there was little impact of charged droplets and ozone on the LB agar nutrient. This is also in agreement with Liu et al's statement regarding the inability of electrical current and charged droplets to affect the nutrients in agar for supporting bacteria growth [1].

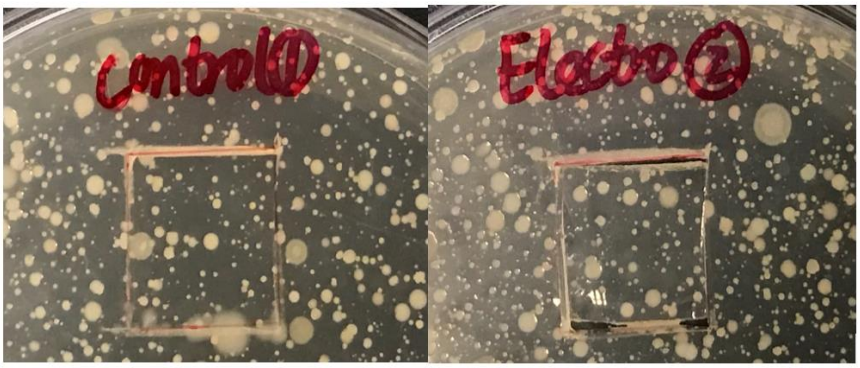

Figure F.1 Effect of electrospray on LB agar nutrient after 22 hours of incubation.

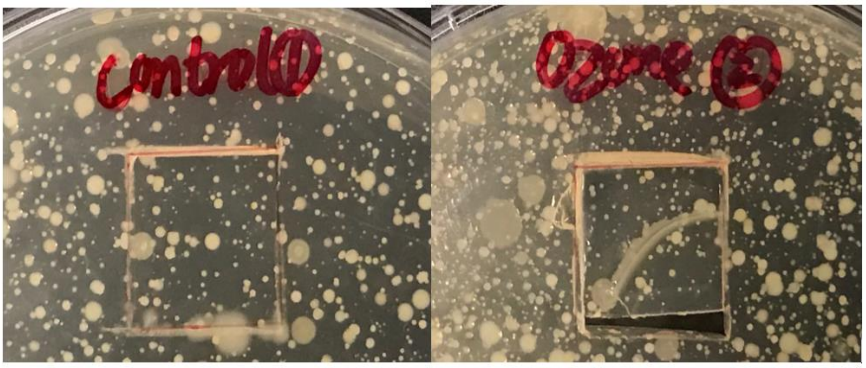

Figure F.2 Effect of ozone on LB agar nutrient after 22 hours of incubation.

F.1 References

[1] Liu, W., Tebbs, S., Byrne, P. and Elliott, T., 1993. The effects of electric current on bacteria colonising intravenous catheters. Journal of Infection, 27(3), pp.261-269.

Appendix G – Swine barn results

The experimental procedures are the same as shown in Chapter 5 except that bacteria were collected in swine barn and the operating condition were selected based on the conclusion in Chapter 6. Figure G.1 clearly demonstrated that the bacteria deactivation efficiency was approximately 97% for 45 min EWNS exposure time. This result indicated that EWNS has shown promising applications in swine barn bacteria deactivation.

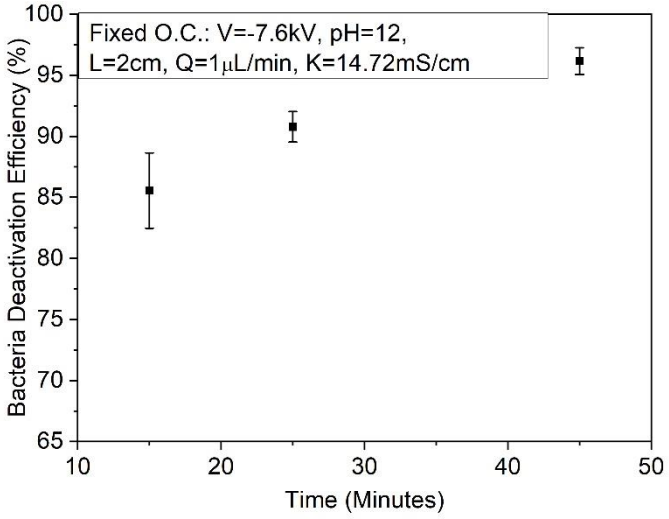

Figure G.1 Effect of EWNS exposure time on swine barn bacteria deactivation efficacy. This employed operating condition: V=-7.6 kV, pH=12, L=2 cm, Q=1 μL/min and K=14.72 mS/cm.